

Bit Allocation using Optimization

Tongda Xu^{1*}, Han Gao^{2,3*}, Chenjian Gao³, Jinyong Pi³, Yanghao Li¹, Yuanyuan Wang³,
Ziyu Zhu¹, Dailan He³, Mao Ye², Hongwei Qin³, Yan Wang^{1†}

¹Tsinghua University, ²University of Electronic Science and Technology of China, ³SenseTime Research
{xutongda, wangyan}@air.tsinghua.edu.cn, {liyangha18, zy-zhu21}@mails.tsinghua.edu.cn,
maoye@uestc.edu.cn, {gaohan1, gaochenjian, pijinyong, wanyuanyuan, hedailan, qinhongwei}@sensetime.com

Abstract

In this paper, we consider the problem of bit allocation in neural video compression (NVC). Due to the frame reference structure, current NVC methods using the same R-D (Rate-Distortion) trade-off parameter λ for all frames are suboptimal, which brings the need for bit allocation. Unlike previous methods based on heuristic and empirical R-D models, we propose to solve this problem by gradient-based optimization. Specifically, we first propose a continuous bit implementation method based on Semi-Amortized Variational Inference (SAVI). Then, we propose a pixel-level implicit bit allocation method using iterative optimization by changing the SAVI target. Moreover, we derive the precise R-D model based on the differentiable trait of NVC. And we show the optimality of our method by proving its equivalence to the bit allocation with precise R-D model. Experimental results show that our approach significantly improves NVC methods and outperforms existing bit allocation methods. Our approach is plug-and-play for all differentiable NVC methods, and it can be directly adopted on existing pre-trained models.

1 Introduction

Neural Video Compression (NVC) has been an active research area. Recently, state-of-the-art (SOTA) NVC approaches (Hu et al. 2022; Li, Li, and Lu 2021) have achieved comparable performance with advanced traditional video coding standards such as H.266 (Bross et al. 2021). The majority of works in NVC focus on improving motion representation (Lu et al. 2019, 2020b; Agustsson et al. 2020) and better temporal context (Djelouah et al. 2019; Lin et al. 2020; Yang et al. 2020; Yilmaz and Tekalp 2021; Li, Li, and Lu 2021). However, the bit allocation of NVC is relatively under-explored (Li et al. 2022).

Due to the frame reference structure of video coding, using the same R-D (Rate-Distortion) trade-off parameter λ for all frames is suboptimal (See Sec. 2.2). Bit allocation is the task of allocating bitrate to different frames/regions according to minimize R-D cost $R + \lambda D$, where R is total bitrate, D is total distortion and λ is the Lagrangian multiplier controlling R-D trade-off. For traditional codecs, bit allocation has been an important topic. Usually, it is jointly considered with bit implementation, and we call the combined pro-

cess bitrate control. Given a video, we first allocate bitrate to frame/block (bit allocation), and then control the encoder to achieve the bitrate (bit implementation). As the optimal bit allocation via exhaustive search is intractable, in practice it is achieved approximately via empirical R-D model (such as q -domain (Lee, Chiang, and Zhang 2000), ρ -domain (He and Mitra 2002; Mao et al. 2021) and λ -domain (Li et al. 2014, 2016, 2020) model) and heuristics modeling of frame/block reference structure (such as mb-tree (Garrett-Glaser 2009) and D- λ model (Li et al. 2016, 2020; Liu and Chen 2021)) (See example in Appendix. A). To simplify notations, in this paper, we use the word R-D model to refer to the actual R-D relationship plus its variants (e.g. R- λ , D- λ , rate/quality dependency models).

The pioneer of bit allocation for NVC (Li et al. 2022) adopts the empirical R- λ model in Li et al. (2014) and proposes a D- λ model based on the frame reference relationship. Like traditional video codec, it relies on empirical models. We show that the Online Encoder Update (OEU) (Lu et al. 2020a) is in fact also a frame-level bit allocation for NVC (See Appendix. B.1-B.2), even though the authors never discuss bit allocation. Other works adopt simplistic heuristics to achieve very coarse bit allocation (Cetin, Yilmaz, and Tekalp 2022).

In this paper, we propose a bit allocation method for NVC using gradient based optimization. It is a new paradigm of bit allocation that is built upon the full differentiability of NVC. It is a pixel-level fine-grained algorithm and does not rely on any empirical R-D model or heuristic. Specifically, we first introduce a bit implementation method based on Semi-Amortized Variational Inference (SAVI) (Kim et al. 2018; Marino, Yue, and Mandt 2018). Then we show that by changing the target of SAVI, we can achieve joint bit allocation and implementation using iterative optimization. More importantly, we show that the precise R-D model of NVC can be computed from the gradient of the decoder, and our approach is equivalent to the bit allocation using the precise R-D model. Thus, it is optimal assuming gradient descent can achieve the global minimum. Our method is compatible with any existing NVC models with a differentiable decoder. And experimental results show that our method significantly improves the R-D performance of SOTA NVC methods (Lu et al. 2019; Li, Li, and Lu 2021) and performs better than existing bit allocation methods (Li et al. 2016, 2022; Lu et al.

*These authors contributed equally.

†Corresponding author.

2020a).

To wrap up, our contributions are as follows:

- We propose bit allocation using optimization. It is a new paradigm of bit allocation based on the end-to-end differentiability of NVC and SAVI. It is the first pixel-level fine-grained bit allocation algorithm and does not rely on any empirical R-D model.
- We construct the precise pixel-level R-D model of NVC using the gradient of NVC decoder. To the best of our knowledge, we are the first to draw a connection between NVC’s gradient and R-D model.
- We further show that our proposed approach is equivalent to the bit allocation using the precise R-D model, which means that our approach is optimal assuming gradient descent achieves the global minimum.
- Our bit allocation method significantly improves SOTA NVC methods, and it outperforms existing bit allocation methods for NVC.
- Our bit allocation method is compatible with any NVC with a differentiable decoder. And it can be directly adopted on existing pre-trained models.

2 Bit Allocation using Optimization

2.1 Background

The majority of NVC follow a mixture of the latent variable model and temporal autoregressive model (Yang et al. 2020). To encode i^{th} frame $\mathbf{x}_i \in \mathbb{R}^{H \times W}$ with $H \times W$ pixels inside a GoP $\mathbf{x}_{1:K}$ with K frames, we first transform the frame to obtain latent parameter $\mathbf{y}_i = f_\phi(\mathbf{x}_i, \mathbf{y}_{<i})$, where $f_\phi(\cdot)$ is the encoder (inference model) parameterized by ϕ , $\lfloor \cdot \rfloor$ is the rounding operator, and $\mathbf{y}_{<i}$ is the quantized latent of previous frames. Then, we obtain $\lfloor \mathbf{y}_i \rfloor$ by quantizing the latent \mathbf{y}_i . Then, an entropy model $p_\theta(\lfloor \mathbf{y}_i \rfloor | \mathbf{y}_{<i})$ parameterized by θ is used to evaluate the probability mass function (pmf, prior) $P_\theta(\lfloor \mathbf{y}_i \rfloor | \mathbf{y}_{<i}) = F_\theta(\lfloor \mathbf{y}_i \rfloor + 0.5 | \mathbf{y}_{<i}) - F_\theta(\lfloor \mathbf{y}_i \rfloor - 0.5 | \mathbf{y}_{<i})$, where F_θ is the cdf of p_θ . With the pmf, we encode $\lfloor \mathbf{y}_i \rfloor$ with bitrate $R_i = -\log P_\theta(\lfloor \mathbf{y}_i \rfloor | \mathbf{y}_{<i})$. During decoding process, we obtain the reconstruction $\hat{\mathbf{x}}_i = g_\theta(\lfloor \mathbf{y}_{\leq i} \rfloor)$, where $g_\theta(\cdot)$ is the decoder (generative model) parameterized by θ . Finally, we compute distortion $D_i = d(\mathbf{x}_i, \hat{\mathbf{x}}_i)$, which can be interpreted as the data likelihood $\log p_\theta(\mathbf{x}_i | \mathbf{y}_{\leq i})$ so long as we treat D_i as energy of Gibbs distribution (Minnen, Ballé, and Toderici 2018). For example, when $d(\cdot, \cdot)$ is MSE, we can interpret $d(\mathbf{x}, \hat{\mathbf{x}}) = -\log p_\theta(\mathbf{x} | \mathbf{y}) + \text{constant}$, where $p_\theta(\mathbf{x} | \mathbf{y}) = \mathcal{N}(\hat{\mathbf{x}}, 1/2\lambda_i I)$. Our optimization target is the per-frame R-D cost (Eq. 1) with Lagrangian multiplier λ controlling R-D trade off. Sometimes, we need to consider pixel-level distortion and the corresponding λ_i . In that case, we denote $\mathbf{D}_i \in \mathbb{R}^{H \times W}$ as the pixel-level distortion vector, then the weighted distortion becomes $\lambda_i^T \mathbf{D}_i$, where $\lambda_i \in \mathbb{R}^{H \times W}$ is the pixel level Lagrangian multiplier.

$$\phi^*, \theta^* \leftarrow \arg \min_{\phi, \theta} R_i + \lambda_i D_i \quad (1)$$

As the rounding operation $\lfloor \cdot \rfloor$ is not differentiable, Ballé, Laparra, and Simoncelli (2016) propose to relax it by additive uniform noise (AUN), and replace $\lfloor \mathbf{y}_i \rfloor$ with $\tilde{\mathbf{y}}_i = \mathbf{y}_i + \mathcal{U}(-1/2, 1/2)$ during training. Under such formulation, we can also treat the above encoding-decoding process as a Variational Autoencoder (Kingma and Welling 2013) on graphic model $\tilde{\mathbf{y}}_{\leq i} \rightarrow \mathbf{x}_i$ with variational posterior $q_\phi(\tilde{\mathbf{y}}_i | \mathbf{x}_i, \tilde{\mathbf{y}}_{<i}) = \mathcal{U}(\mathbf{y}_i - 1/2, \mathbf{y}_i + 1/2)$. And then minimizing the uniform noise relaxed R-D cost (Eq. 1) is equivalent to maximizing the evident lowerbound (ELBO) (Eq. 2) by Stochastic Gradient Variational Bayes-A (SGVB-A) (Kingma and Welling 2013).

$$\mathcal{L}_i = \mathbb{E}_{q_\phi(\tilde{\mathbf{y}}_i | \mathbf{x}_i, \tilde{\mathbf{y}}_{<i})} \left[\underbrace{\log P_\theta(\tilde{\mathbf{y}}_i | \tilde{\mathbf{y}}_{<i})}_{-R_i} + \underbrace{\log p_\theta(\mathbf{x}_i | \tilde{\mathbf{y}}_{\leq i})}_{\lambda D_i} - \underbrace{\log q_\phi(\tilde{\mathbf{y}}_i | \mathbf{x}_i, \tilde{\mathbf{y}}_{<i})}_0 \right] \quad (2)$$

2.2 Why Bit Allocation is Necessary

In this section, we explain why bit allocation is necessary for video compression, but not for image compression. First, let’s consider the task of compressing $\mathbf{x}_{1:K}$ with a overall R-D trade-off parameter λ_0 . Then the target of bit allocation is to minimize the overall R-D cost in Eq. 3 by adjusting the pixel-level R-D trade-off parameter λ_i (Eq. 3). And by setting the gradient of Eq. 1 and Eq. 3 to 0, we have Eq. 4 and Eq 5 hold for optimal bit allocation, where $\lambda_0 = \{\lambda_0, \dots, \lambda_0\}^{H \times W}$.

$$\lambda_1^*, \dots, \lambda_k^* \leftarrow \arg \min_{\lambda_1, \dots, \lambda_k} \sum_{i=1}^K R_i + \lambda_0 \sum_{i=1}^K D_i \quad (3)$$

$$\sum_{j=1}^K \frac{\partial R_j}{\partial \lambda_i} + \lambda_0^T \sum_{j=1}^K \frac{\partial D_j}{\partial \lambda_i} = 0 \quad (4)$$

$$\lambda_i^T + \frac{\partial R_i}{\partial D_i} = 0 \quad (5)$$

Consider now we compress each \mathbf{x}_i independently. Then the λ_i is irrelevant to the rate and distortion of j^{th} image (Eq. 6). Taking Eq. 6 and Eq. 5 into Eq. 4, we have $\lambda_i^* = \lambda_0$. In other words, the R-D cost of independent image compression is optimal when every image \mathbf{x}_i is encoded with the same λ_0 .

$$\frac{\partial R_{j \neq i}}{\partial \lambda_i} = 0, \frac{\partial D_{j \neq i}}{\partial \lambda_i} = 0 \quad (6)$$

However, for video compression, Eq. 6 does not hold in general as previous frame’s encoding result effects current frame. And assuming $\lambda_i^* = \lambda_0$, we have Eq. 6 holds, which brings contradiction. In other words, when encoding a GoP with inter-frame dependency, encoding each frame and region with the same λ_0 is suboptimal. And this is the essential reason why bit allocation is necessary.

One may argue that for NVC, we can directly use the GoP level optimization target (Eq. 3) for training. In fact, this is known as cascaded loss (Lu et al. 2020a; Sheng et al. 2021) and it can improve the R-D performance of NVC to some extent. However, this improvement comes from reducing dataset shifting instead of bit allocation. During the actual sequential encoding process, the encoder has no idea about the current frame x_i 's impact upon later frames inside the GoP. Thus, it is not possible to allocate bit to different frame/area according to frame reference structure.

2.3 Bit Implementation using Semi-Amortized Variational Inference

Usually a bit implementation method that can achieve continuous R-D trade-off is necessary to realize the result of bit allocation. Existing continuous bit implementation approaches for NVC (Lin et al. 2021b,a) stem from variable bitrate image compression (Choi, El-Khamy, and Lee 2019). In this section, we provide an alternative bit implementation method based on Semi-Amortized Variational Inference (SAVI) (Kim et al. 2018; Marino, Yue, and Mandt 2018), which can be further extended into an implicit bit allocation as we describe in Sec. 2.4.

Consider we have a pair of encoder-decoder parameter $\phi_{\lambda_0}, \theta_{\lambda_0}$ which is optimized under a specific λ_0 . Our target is to encode frame x_i with a different R-D trade-off parameter $\lambda_i \in \mathbb{R}^{H \times W}$, which is a pixel-level bit allocation map. And this frame has to be decodable with decoder parameter θ_{λ_0} . Consider given a frame x_i , we run the encoder once to obtain y_i . Then following Choi, El-Khamy, and Lee (2019), we augment the pmf with quantization step-size Δ . Denote the dequantized latent $\lfloor y_i / \Delta_i \rfloor \Delta_i$ as $\lfloor y_i \rfloor_{\Delta_i}$, then the new pmf $P_{\theta_{\lambda_0}}(\lfloor y_i / \Delta_i \rfloor \lfloor y_{<i} \rfloor_{\Delta_{<i}}) = F_{\theta_{\lambda_0}}(\lfloor y_i \rfloor_{\Delta_i} + \Delta_i/2 \lfloor y_{<i} \rfloor_{\Delta_{<i}}) - F_{\theta_{\lambda_0}}(\lfloor y_i \rfloor_{\Delta_i} - \Delta_i/2 \lfloor y_{<i} \rfloor_{\Delta_{<i}})$. And then iteratively, we directly optimize y_i and Δ_i by gradient descent as Eq. 7-8. In fact, this method is a simplified form of SAVI. As we first initialize the variational posterior parameter y_i with fully amortized variational inference, and then directly optimize variational posterior for each data point by stochastic gradient descent. The word amortized means that for all the data points x_i , we have only one encoder parameter ϕ_{λ_0} . Previous works (Djelouah and Schroers 2019; Yang, Bamler, and Mandt 2020; Zhao et al. 2021) adopt similar method to improve R-D performance of NIC. However, to the best of our knowledge, we are the first to conduct bit implementation of NVC by SAVI.

$$y_i^*, \Delta_i^* \leftarrow \arg \max_{y_i, \Delta_i} \mathcal{L}_i^{BI} \quad (7)$$

$$\begin{aligned} \mathcal{L}_i^{BI} = & \log P_{\theta_{\lambda_0}}(\lfloor y_i / \Delta_i \rfloor \lfloor y_{<i} \rfloor_{\Delta_{<i}}) \\ & - \lambda_i^T d(x, g_{\theta_{\lambda_0}}(\lfloor y_{\leq i} \rfloor_{\Delta_{\leq i}})) \end{aligned} \quad (8)$$

As the rounding operator $\lfloor \cdot \rfloor$ is not differentiable, we extend the Stochastic Gumbel Annealing (SGA) (Yang, Bamler, and Mandt 2020) to support Δ_i and compute path-wise gradient (Mohamed et al. 2020).

2.4 Implicit Bit Allocation

Previous works in bit allocation (Li et al. 2016, 2022) solve per-frame/block λ_i as bit allocation map explicitly. If we explicitly solve the per-pixel bit allocation map λ_i for frame x_i , we can achieve it with the bit implementation method above. However, this 2-stage approach is unnecessary. In fact, we can achieve optimal bit allocation implicitly by simply changing the target of our bit implementation. Then we can jointly achieve bit allocation and implementation by optimization.

Consider a surprisingly simple modification of Eq. 8. Instead of optimizing the per-frame y_i, Δ_i towards an external pixel level map λ_1 , we optimize the $y_{1:K}, \Delta_{1:K}$ of the whole GoP towards the overall R-D cost of the GoP as Eq. 4, with distortion weighted by the original Lagrangian multiplier λ_0 . This results in an optimization objective as Eq. 9-10. It is an implicit bit allocation as no λ_i is explicitly solved. In the rest of this Sec., Sec. 2.5 and Sec. 2.6, we show that it is the optimal bit allocation given gradient descent achieves global minimum.

$$y_{1:K}^*, \Delta_{1:K}^* \leftarrow \arg \max_{y_{1:K}, \Delta_{1:K}} \mathcal{L}^{BA} \quad (9)$$

$$\begin{aligned} \mathcal{L}^{BA} = & \sum_i^K \underbrace{\log P_{\theta_{\lambda_0}}(\lfloor y_i / \Delta_i \rfloor \lfloor y_{<i} \rfloor_{\Delta_{<i}})}_{-R_i} \\ & - \lambda_0 \sum_i^K \underbrace{d(x, g_{\theta_{\lambda_0}}(\lfloor y_{\leq i} \rfloor_{\Delta_{\leq i}}))}_{D_i} \end{aligned} \quad (10)$$

To understand why our approach is optimal, let's revisit the computational graph defined by decoding sequence of NVC using P frames. To simplify notations, we treat y_i as a concatenation of y_i and Δ_i . As show in Fig. 1(a), if we compute the gradient of $R_{i+1} + \lambda_0 D_{i+1}$, the gradient automatically flows back to the latent representation of y_i that $i + 1^{th}$ frame refers to, and even back to the latent representation of the very first frame. Formally, the gradient of i^{th} frame's latent y_i with regard to \mathcal{L}^{BA} in Eq. 10 can be split into two part as Eq. 11.

$$\frac{\partial \mathcal{L}^{BA}}{\partial y_i} = \underbrace{\frac{\partial (R_i + \lambda_0 D_i)}{\partial y_i}}_{\text{Part I}} - \underbrace{\sum_{j=i+1}^K \frac{\partial (R_j + \lambda_0 D_j)}{\partial y_i}}_{\text{Part II}} \quad (11)$$

The Part I gradient is pushing the i^{th} frame towards minimizing $R_i + \lambda_0 D_i$, which is suboptimal as we discussed in Sec. 2.2. The Part II gradient, which is the gradient of other frame referring to i^{th} frame, is pushing i^{th} frame away from minimizing $R_i + \lambda_0 D_i$. When combined together, the target is to optimize the overall R-D cost in Eq. 3. In fact, we can construct a pixel-level bit allocation map λ'_i to make minimizing $R_i + \lambda_i'^T D_i$ equivalent to maximizing \mathcal{L}^{BA} in Eq. 10. We call λ'_i the equivalent explicit bit allocation map. As it is the explicit bit allocation map that is equivalent to

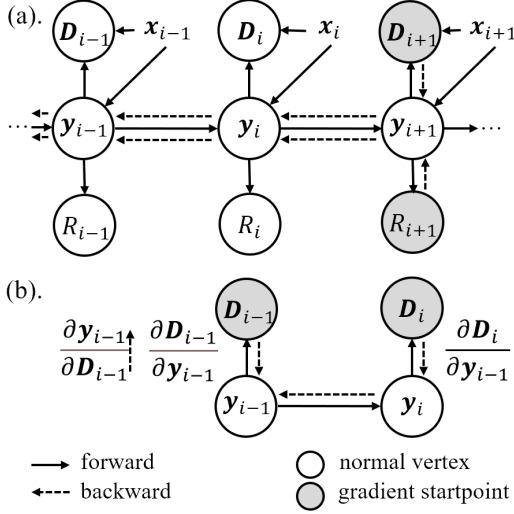


Figure 1: (a). The computational graph defined by NVC using P frames under Asm. 1. If we take gradient of D_{i+1}, R_{i+1} , the gradient naturally flows back to previous latent $\mathbf{y}_{\leq i}$. (b). An example of how to compute $\partial D_i / \partial D_{i-1}$. As no path exists from D_i to D_{i-1} , we need to find their lowest common ancestor \mathbf{y}_{i-1} as intermediate, compute $\partial D_{i-1} / \partial \mathbf{y}_{i-1}$ and $\partial D_i / \partial \mathbf{y}_i$, and obtain the $\partial \mathbf{y}_{i-1} / \partial D_{i-1}$ by taking element-wise reciprocal of Jacobian $\partial D_{i-1} / \partial \mathbf{y}_{i-1}$ to create a fake edge to allow gradient flow back from \mathbf{y}_{i-1} to D_{i-1} .

our implicit bit allocation algorithm. In Sec. 2.5, we solve λ'_i . In Sec. 2.6, we show the optimality of our approach by proving that λ'_i is equivalent to the direct bit allocation map λ_i^* solved by Eq. 3.

2.5 Equivalent Explicit Bit Allocation

As stated above, the equivalent explicit bit allocation map λ'_i is constructed to make minimizing $R_i + \lambda_i'^T D_i$ equivalent to maximizing \mathcal{L}^{BA} , which means that their gradient with regard to \mathbf{y}_i is the additive inverse (Eq. 13). Formally, under the common mild assumption (Li et al. 2016, 2022):

Assumption 1. *The frame i does not influence frame j directly, but in a frame-by-frame manner.*

, we have the following theorem:

Theorem 1. *Under Asm. 1, for NVC with P frames, let*

$$\lambda'_i = \left(1 + \sum_{j=i+1}^K \prod_{k=i+1}^j \frac{\partial D_k}{\partial D_{k-1}}\right)^T \lambda_0 / \left(1 + \sum_{j=i+1}^K \prod_{k=i+1}^j \frac{\partial R_k}{\partial R_{k-1}}\right) \quad (12)$$

, then λ'_i satisfies:

$$-\frac{\partial (R_i + \lambda_i'^T D_i)}{\partial \mathbf{y}_i} = \frac{\partial \mathcal{L}^{BA}}{\partial \mathbf{y}_i} \quad (13)$$

, where $\partial D_k / \partial D_{k-1}, \partial R_k / \partial R_{k-1}$ can be computed numerically through the gradient of NVC.

Proof. To find λ'_i , we need to represent $\partial R_j / \partial \mathbf{y}_i, \partial D_j / \partial \mathbf{y}_i$ in Eq. 11 with R_i, D_i . To achieve this, we expand $\partial R_j / \partial \mathbf{y}_i, \partial D_j / \partial \mathbf{y}_i$ as Eq. 14. However, as shown in Fig. 1, the gradient $\partial R_k / \partial R_{k-1}, \partial D_k / \partial D_{k-1}$ required by Eq. 14 can not be computed directly as they are siblings in the computational graph (Fig. 1). Instead, we need to find their lowest common ancestor \mathbf{y}_{k-1} as an intermediate variable and further expand them as Eq. 15. Note that the gradient $\partial R_k / \partial \mathbf{y}_{k-1}, \partial D_k / \partial \mathbf{y}_{k-1}$ can be easily obtained as a path exists from \mathbf{y}_k to R_k, D_k in the computational graph. From the definition of Jacobian, we can numerically obtain the reverse direction gradient $\partial \mathbf{y}_{k-1} / \partial R_{k-1}, \partial \mathbf{y}_{k-1} / \partial D_{k-1}$ by taking reciprocal of each element of the Jacobian $\partial R_{k-1} / \partial \mathbf{y}_{k-1}, \partial D_{k-1} / \partial \mathbf{y}_{k-1}$ as Eq. 16. In this way, we can represent $\partial R_j / \partial \mathbf{y}_i, \partial D_j / \partial \mathbf{y}_i$ by $\partial R_i / \partial \mathbf{y}_i, \partial D_i / \partial \mathbf{y}_i$. In fact, as we show in Sec. 2.6, we are actually computing the precise R-D model of NVC.

$$\begin{aligned} \frac{\partial R_j}{\partial \mathbf{y}_i} &= \prod_{k=i+1}^j \frac{\partial R_k}{\partial R_{k-1}} \frac{\partial R_i}{\partial \mathbf{y}_i} \\ \frac{\partial D_j}{\partial \mathbf{y}_i} &= \prod_{k=i+1}^j \frac{\partial D_k}{\partial D_{k-1}} \frac{\partial D_i}{\partial \mathbf{y}_i} \end{aligned} \quad (14)$$

$$\begin{aligned} \frac{\partial R_k}{\partial R_{k-1}} &= \frac{\partial R_k}{\partial \mathbf{y}_{k-1}} \frac{\partial \mathbf{y}_{k-1}}{\partial R_{k-1}} \\ \frac{\partial D_k}{\partial D_{k-1}} &= \frac{\partial D_k}{\partial \mathbf{y}_{k-1}} \frac{\partial \mathbf{y}_{k-1}}{\partial D_{k-1}} \end{aligned} \quad (15)$$

$$\begin{aligned} \left(\frac{\partial \mathbf{y}_{k-1}}{\partial R_{k-1}}\right)^{mn} &= 1 / \left(\frac{\partial R_{k-1}}{\partial \mathbf{y}_{k-1}}\right)^{nm} \\ \left(\frac{\partial \mathbf{y}_{k-1}}{\partial D_{k-1}}\right)^{mn} &= 1 / \left(\frac{\partial D_{k-1}}{\partial \mathbf{y}_{k-1}}\right)^{nm} \end{aligned} \quad (16)$$

Taking Eq. 14 into Eq. 11, we obtain the gradient of \mathcal{L}^{BA} as Eq. 17. And by reorganizing Eq. 17 into the form of $-\partial R_i / \partial \mathbf{y}_i - \lambda_i'^T D_i / \partial \mathbf{y}_i$, we can solve our equivalent bit allocation map λ'_i as Eq. 12, which completes the proof.

$$\begin{aligned} \frac{\partial \mathcal{L}^{BA}}{\partial \mathbf{y}_i} &= - \left(1 + \sum_{j=i+1}^K \prod_{k=i+1}^j \frac{\partial R_k}{\partial R_{k-1}}\right) \frac{\partial R_i}{\partial \mathbf{y}_i} \\ &\quad - \lambda_0^T \left(1 + \sum_{j=i+1}^K \prod_{k=i+1}^j \frac{\partial D_k}{\partial D_{k-1}}\right) \frac{\partial D_i}{\partial \mathbf{y}_i} \end{aligned} \quad (17)$$

□

We note that λ'_i in Eq. 12 is a quotient: the dividend has the form of a pixel-level re-weighted λ_0 , and the divisor has the form of a normalization scalar. And when $i = K$, $\lambda_i = \lambda_0$. Note that the general case beyond P frames is more complicated, which is discussed in Appendix C.2.

Although we can solve λ'_i , the practical computational cost is extremely high due to the size of the Jacobian matrix. For example, for a video with 256×256 pixels encoded with (Lu et al. 2019), $\partial \mathbf{D}_j / \partial \mathbf{y}_i$ requires around 77 gigabytes memory to store. Luckily, we never need to compute the explicit bit allocation map λ'_i to conduct implicit bit allocation.

2.6 Precise R-D model and Optimality

From traditional bit allocation’s perspective, the $\partial R_k / \partial R_{k-1}, \partial \mathbf{D}_k / \partial \mathbf{D}_{k-1}$ of Eq. 14 plays the role of the R-D model. In fact, in Li et al. (2016), the $\partial R_k / \partial R_{k-1}$ is called rate dependency model, and $\partial \mathbf{D}_k / \partial \mathbf{D}_{k-1}$ is called quality dependency model. They are the fundamental R-D models for bit allocation. While in traditional bit allocation methods, those important relationships are described by simple empirical models. For example, Li et al. (2016) empirically model $\partial R_k / \partial R_{k-1} \approx 0$ and $\partial \sum_{k=i}^K \mathbf{D}_k / \partial \mathbf{D}_i$ as constant. And Li et al. (2022) empirically model $\partial \mathbf{D}_k / \partial \mathbf{D}_{k-1}$ as constant. For us, the $\partial R_k / \partial R_{k-1}, \partial \mathbf{D}_k / \partial \mathbf{D}_{k-1}$ are accurately computed through Jacobian. They reflect the precise pixel-level frame reference relationship without any empirical assumption or simplification.

In fact, Eq. 15 describes the precise underlying R-D model behind NVC based on gradient. And with the accurate R-D model, we can also directly solve λ_i^* for optimal bit allocation from Eq. 3, with λ_i as optimization target instead of \mathbf{y}_i . Moreover, this directly solved λ_i^* is the same as λ'_i :

Theorem 2. *Under Asm. 1, given the precise R-D model as Eq. 15, the bit allocation map λ_i^* directly solved from Eq. 3 equals to the explicit equivalent bit allocation map of the proposed implicit bit allocation algorithm. In other words, $\lambda_i^* = \lambda'_i$.*

Proof. See Appendix. C.1 □

Thm. 2 shows that our implicit bit allocation is equivalent to direct bit allocation using the exact R-D model, which in turn proves the optimality of our approach.

Moreover, our bit allocation is a generalization of other λ -domain bit allocation. By forcing $\partial R_k / \partial R_{k-1} = 0$ in Eq. 12 and setting $\partial \mathbf{D}_k / \partial \mathbf{D}_{k-1}$ to simplified empirical models, our λ'_i has same form as the bit allocation map solved in Li et al. (2016), Li et al. (2020) and Li et al. (2022) (See Appendix. A for details).

2.7 Entropy Coding and Bitstream Specification

We adopt the *torchac*’s (Mentzer et al. 2019) implementation of arithmetic coding to encode and decode $\lfloor \mathbf{y}_i / \Delta_i \rfloor$. And as Choi, El-Khany, and Lee (2019), we directly store Δ_i as a 32 bit float since its bitrate is negligible.

3 Related Work

3.1 Bit Allocation for Video Compression

Bit allocation is an important topic for traditional video codec. The core of bit allocation is to construct an empirical R-D model that captures the R-D relationship between

dependent frames. Since early development of video codec, various empirical models have been developed, such as q -domain model (Lee, Chiang, and Zhang 2000), ρ -domain model (He and Mitra 2002), λ -domain model (Li et al. 2014, 2016; Liu and Chen 2021) and even Taylor expansion based model (Li et al. 2017). Among them the λ -domain model performs the best, and has been widely adopted in advanced standards such as H.265 and H.266. We give a detailed review of λ -domain bit allocation (Li et al. 2016) in Appendix. A.

The pioneer of bit allocation for NVC (Li et al. 2022) designs a D- λ model to the trait of NVC. While it is still an empirical R-D model and ignores the precise R-D model defined by gradient. Other recent works that consider the bit allocation for NVC only adopt simple heuristic such as insert 1 high quality frame per 4 frames (Hu et al. 2022; Cetin, Yilmaz, and Tekalp 2022). However, we find that a relatively old work in 2020 (Lu et al. 2020a) is actually a frame-level bit allocation for NVC, even though the authors never realize it and have not mentioned bit allocation at all. In Appendix. B.1-B.2, we give a detailed discussion about why it is a frame-level bit allocation, and how it is related to our work.

3.2 Semi-Amortized Inference for Neural Codec

The Semi-Amortized Variational Inference (SAVI) is proposed by Kim et al. (2018); Marino, Yue, and Mandt (2018). The idea is that the inference model (encoder) parameter ϕ is froze once after training. In testing time this parameter is fully amortized by all future data, and this leads to sub-optimal inference results (Cremer, Li, and Duvenaud 2018). The SAVI initializes the parameter of variational posterior as the output of inference network, and then optimizes the parameter iteratively per data-point.

The original SAVI requires a 2-stage optimization between every gradient descent step. When applying SAVI to neural codec with practically large model, people limit it to the final inference stage only. Prior works Djelouah and Schroers (2019); Yang, Bamler, and Mandt (2020); Zhao et al. (2021) adopt SAVI to improve R-D performance in neural image compression. And to the best of our knowledge, we are the first to extend SAVI to bit allocation and bit implementation in NVC.

4 Experimental Results

4.1 Experimental Settings

All the code is implemented in PyTorch 1.9 and CUDA 11.2, and the experiments are conducted on a computer with AMD(R) EPYC 7742 Processor and $8 \times$ NVIDIA(R) A100. Following other works in NVC (Lu et al. 2019; Li, Li, and Lu 2021), we adopt HEVC Common Testing Condition (CTC) (Bossen et al. 2013) and UVG dataset (Mercat, Viitanen, and Vanne 2020) to test our method. And the GoP size is set to 10 for HEVC CTC and 12 for UVG dataset. The R-D performance is measured by Bjontegaard-Bitrate (BD-BR) and BD-PSNR (Bjontegaard 2001). For both of the baseline methods (Lu et al. 2019; Li, Li, and Lu 2021), we

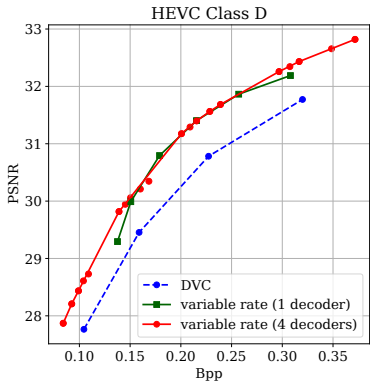


Figure 2: Experimental result of variable bitrate coding.

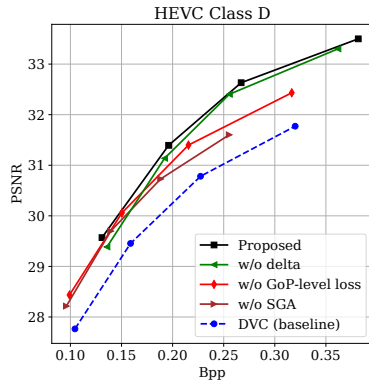


Figure 3: Ablation study result of bit allocation.

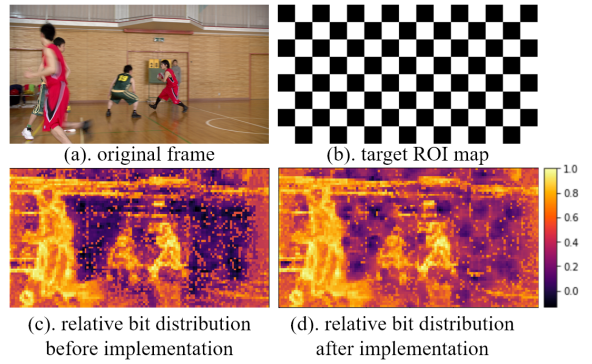


Figure 4: Experimental result of pixel-level bit implementation. See more in Appendix. D.3.

adopt the official pre-trained models. For I frame compression, we adopt Cheng et al. (2020) with pre-trained models provided by Bégaïnt et al. (2020). For the proposed bit implementation and allocation, we adopt Adam optimizer with $lr = 1 \times 10^{-3}$. And for each GoP we optimize $\mathbf{y}_{1:K}, \Delta_{1:K}$ for 2000 iterations. More implementation details are presented in Appendix. D.1-D.2.

4.2 Bit Implementation

In this section, we empirically verify the ability of the method proposed in Sec. 2.3 to achieve pixel level bit implementation.

Variable Bitrate Coding First, we test the ability of our proposed method to span the whole R-D curve with countable decoders. The green line in Fig. 2 shows that our method can achieve bitrate in a large range (0.14–0.31 bpp) with only 1 decoder. And the red line in Fig. 2 shows that our method can span the whole R-D curve (0.08–0.37 bpp) with 4 decoders (See more in Appendix. D.3).

Pixel-level Bit Implementation Fig. 4 shows the ability of our method in implementing the bitrate according to a checkerboard λ map $\in \mathbb{R}^{H \times W}$, which is a matrix filled with 0 and λ . Bit distribution result verifies that our proposed method can allocate bit spatially according to an external bit allocation map.

4.3 Bit Allocation

In this section, we show the R-D performance of our proposed bit allocation method and provide insights about why it works through ablation study and analysis.

R-D Performance of Proposed Bit Allocation In Tab. 1 and Fig. 5, we show the R-D performance of our approach compared with baseline methods (Lu et al. 2019; Li, Li, and Lu 2021) (w/o bit allocation) and other bit allocation methods (Li et al. 2016, 2022; Lu et al. 2020a). Li et al. (2016) is a traditional frame-level bit allocation method that is directly adopted to NVC. Li et al. (2022) is the first bit allocation algorithm that is intentionally designed for NVC. And we include the OEU (Lu et al. 2020a) as we recognise it as a frame-level bit allocation.

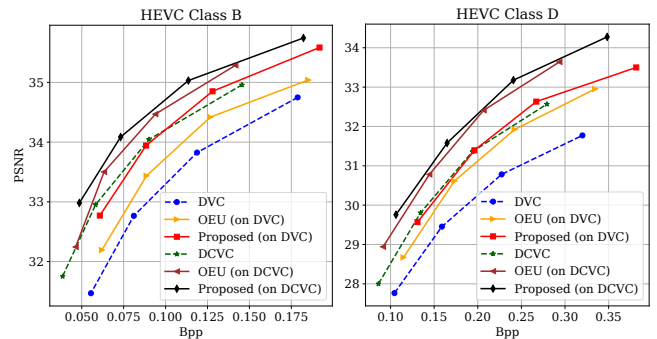


Figure 5: The R-D performance of our bit allocation compared with baselines (w/o bit allocation) and OEU. See HEVC Class C/E and UVG in Appendix. D.4.

Tab. 1 shows that our proposed bit allocation method significantly improves the BD-BR and BD-PSNR over two baseline methods (w/o bit allocation). Specifically, our bit allocation achieves BD-BR of approximately -25% for DVC (Lu et al. 2019) and -20% for DCVC (Li, Li, and Lu 2021). Moreover, our approach outperforms all other bit allocation approaches. It is also interesting to note that despite the OEU (Lu et al. 2020a) is earlier than Li et al. (2022), its R-D performance is significantly better than the later.

Qualitative Results, Entropy Coding and Error Bar

See Appendix D.4.

Ablation Study Effect of Δ and SGA When performing SAVI, we add quantization step size Δ with latent \mathbf{y} into optimization parameters. Moreover, we adopt SGA instead of AUN as continuous relaxation of quantization. The green line in Fig. 3 shows that removing Δ marginally degrades the R-D performance. The brown line in Fig. 3 shows that substituting SGA with AUN significantly harms the R-D performance.

Effect of Optimization Target Our method is only a valid bit allocation with GoP level R-D cost (Eq. 10). With optimization target changed into frame-level R-D cost (Eq. 8), the remaining gain comes from the elimination of the

Method	BD-BR (%) ↓					BD-PSNR (dB) ↑				
	Class B	Class C	Class D	Class E	UVG	Class B	Class C	Class D	Class E	UVG
<i>DVC (Lu et al. 2019) as Baseline</i>										
Li et al. (2016)*	20.21	17.13	13.71	10.32	16.69	-0.54	-	-	-0.32	-0.47
Li et al. (2022)*	-6.80	-2.96	0.48	-6.85	-4.12	0.19	-	-	0.28	0.14
OEU (Lu et al. 2020a)	-13.57	-11.29	-18.97	-12.43	-13.78	0.39	0.49	0.83	0.48	0.48
Proposed	-28.55	-26.82	-25.37	-32.54	-27.68	0.87	1.11	1.17	1.35	0.98
<i>DCVC (Li, Li, and Lu 2021) as Baseline</i>										
OEU (Lu et al. 2020a)	-10.75	-14.34	-16.30	-7.15	-16.07	0.30	0.58	0.74	0.29	0.50
Proposed	-20.59	-19.69	-20.60	-23.33	-25.22	0.52	0.76	0.96	0.96	0.69

Table 1: The BD-BR and BD-PSNR of our approach compared with baselines (w/o bit allocation) and other bit allocation approaches. The data with * comes from Li et al. (2022), and all other data are reproduced by authors. We mark some data with '-' as they are not reported by Li et al. (2022). The difference in I frames brings a small gap between the OEU's reproduced R-D performance and reported in Lu et al. (2020a) (See Appendix. B.3 for details).

amortization gap (Cremer, Li, and Duvenaud 2018; Yang, Bamler, and Mandt 2020). And as shown of the red line in Fig. 3, changing the optimization target to the per-frame R-D cost significantly harms the R-D performance.

Effect of GoP Size Tab. 2 shows the BD-BR and BD-PSNR of the proposed method compared with baseline (w/o bit allocation) at GoP size $\{4, 10, 16, 32\}$. It can be observed that the benefit of our approach saturates at GoP size 16. It is somehow surprising that the gain brought by our method does not grow with GoP size consistently. It could be the numerical problem of optimization that is brought by gradient accumulation.

GoP Size	BD-BR(%) ↓	BD-PSNR(dB) ↑
K=4	-21.97	1.08
K=10	-25.37	1.17
K=16	-26.90	1.17
K=32	-23.90	0.88

Table 2: Effect of GoP size K on R-D performance of our proposed method on HEVC Class D dataset.

Analysis on Bit Allocation Results In this section, we visualize the result of our bit allocation to formulate an intuitive idea about what does bit allocation do on earth. From Fig. 6, we can see that the bitrate of the regions that are not referred to is relatively reduced by bit allocation, which is aligned with intuition.

Analysis on How Metric Changes with Frame Index See how distortion, bitrate and R-D cost change with frame index before and after bit allocation in Appendix. D.5.

5 Conclusion

We propose a novel paradigm of bit allocation method for NVC by SAVI. Unlike previous methods, it is a fine-grained pixel level method without any empirical R-D model. Moreover, we show its optimality by proofing its equivalence to

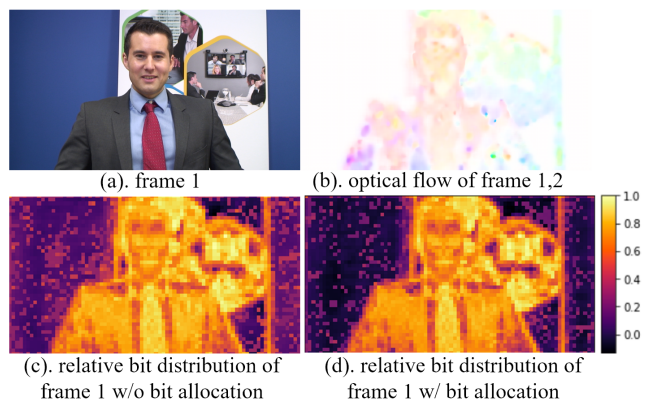


Figure 6: The bit rate distribution before/after bit allocation of *Johnny* in HEVC Class E. See more in Appendix. D.5.

the bit allocation using exact R-D models. And empirical results verify the effectiveness of the proposed approach.

6 Limitations

The major limitation of our method is encoding complexity. Although the decoding time is not influenced, our method requires iterative gradient descent during encoding. Practically, our approach is limited to scenarios when R-D performance matters more than encoding time (e.g. content delivery network). Or it can also be used as an empirical R-D lower-bound for research on faster bit allocation methods.

See more discussions and social impact in Appendix. E.

References

- Agustsson, E.; Minnen, D.; Johnston, N.; Balle, J.; Hwang, S. J.; and Toderici, G. 2020. Scale-space flow for end-to-end optimized video compression. In *Proc. IEEE Comput. Soc. Conf. Comput. Vis. Pattern Recognit.*, 8503–8512.
- Ballé, J.; Laparra, V.; and Simoncelli, E. P. 2016. End-to-end optimized image compression. *arXiv preprint arXiv:1611.01704*.
- Ballé, J.; Minnen, D.; Singh, S.; Hwang, S. J.; and Johnston, N.

2018. Variational image compression with a scale hyperprior. In *Int. Conf. on Learning Representations*.
- Bégaint, J.; Racapé, F.; Feltman, S.; and Pushparaja, A. 2020. CompressAI: a PyTorch library and evaluation platform for end-to-end compression research. *arXiv preprint arXiv:2011.03029*.
- Bjontegaard, G. 2001. Calculation of average PSNR differences between RD-curves. *VCEG-M33*.
- Bossen, F.; et al. 2013. Common test conditions and software reference configurations. *JCTVC-L1100*, 12(7).
- Bross, B.; Chen, J.; Ohm, J.-R.; Sullivan, G. J.; and Wang, Y.-K. 2021. Developments in international video coding standardization after avc, with an overview of versatile video coding (vvc). *Proc. IEEE*, 109(9): 1463–1493.
- Cetin, E.; Yılmaz, M. A.; and Tekalp, A. M. 2022. Flexible-Rate Learned Hierarchical Bi-Directional Video Compression With Motion Refinement and Frame-Level Bit Allocation. *arXiv e-prints*, arXiv–2206.
- Cheng, Z.; Sun, H.; Takeuchi, M.; and Katto, J. 2020. Learned image compression with discretized gaussian mixture likelihoods and attention modules. In *Proc. IEEE Comput. Soc. Conf. Comput. Vis. Pattern Recognit*, 7939–7948.
- Choi, Y.; El-Khamy, M.; and Lee, J. 2019. Variable Rate Deep Image Compression With a Conditional Autoencoder. In *Proc. IEEE Int. Conf. Comput. Vis.*, 3146–3154. IEEE.
- Cremer, C.; Li, X.; and Duvenaud, D. 2018. Inference suboptimality in variational autoencoders. In *Int. Conf. on Machine Learning*, 1078–1086. PMLR.
- Djelouah, A.; Campos, J.; Schaub-Meyer, S.; and Schroers, C. 2019. Neural Inter-Frame Compression for Video Coding. In *Proc. IEEE Int. Conf. Comput. Vis.*
- Djelouah, J. C. M. S. A.; and Schroers, C. 2019. Content Adaptive Optimization for Neural Image Compression. In *Proc. IEEE Comput. Soc. Conf. Comput. Vis. Pattern Recognit*.
- Garrett-Glaser, J. 2009. A novel macroblock-tree algorithm for high-performance optimization of dependent video coding in H. 264/AVC. *Tech. Rep.*
- He, Z.; and Mitra, S. K. 2002. Optimum bit allocation and accurate rate control for video coding via ρ -domain source modeling. *IEEE Trans. Circuits Syst. Video Technol.*, 12(10): 840–849.
- Hu, Z.; Lu, G.; Guo, J.; Liu, S.; Jiang, W.; and Xu, D. 2022. Coarse-To-Fine Deep Video Coding With Hyperprior-Guided Mode Prediction. In *Proc. IEEE Comput. Soc. Conf. Comput. Vis. Pattern Recognit*, 5921–5930.
- Kim, Y.; Wiseman, S.; Miller, A.; Sontag, D.; and Rush, A. 2018. Semi-amortized variational autoencoders. In *Int. Conf. on Machine Learning*, 2678–2687. PMLR.
- Kingma, D. P.; and Welling, M. 2013. Auto-encoding variational bayes. *arXiv preprint arXiv:1312.6114*.
- Lee, H.-J.; Chiang, T.; and Zhang, Y.-Q. 2000. Scalable rate control for MPEG-4 video. *IEEE Trans. Circuits Syst. Video Technol.*, 10(6): 878–894.
- Li, B.; Li, H.; Li, L.; and Zhang, J. 2014. λ domain rate control algorithm for High Efficiency Video Coding. *IEEE Trans. Image Process.*, 23(9): 3841–3854.
- Li, J.; Li, B.; and Lu, Y. 2021. Deep contextual video compression. *Advances in Neural Information Processing Systems*, 34.
- Li, L.; Li, B.; Li, H.; and Chen, C. W. 2016. λ -domain optimal bit allocation algorithm for High Efficiency Video Coding. *IEEE Trans. Circuits Syst. Video Technol.*, 28(1): 130–142.
- Li, S.; Xu, M.; Wang, Z.; and Sun, X. 2017. Optimal bit allocation for CTU level rate control in HEVC. *IEEE Trans. Circuits Syst. Video Technol.*, 27(11): 2409–2424.
- Li, Y.; Chen, X.; Li, J.; Wen, J.; Han, Y.; Liu, S.; and Xu, X. 2022. Rate Control for Learned Video Compression. In *ICASSP 2022-2022 IEEE Int. Conf. on Acoustics, Speech and Signal Processing (ICASSP)*, 2829–2833. IEEE.
- Li, Y.; Liu, Z.; Chen, Z.; and Liu, S. 2020. Rate control for versatile video coding. In *IEEE Int. Conf. on Image Process.*, 1176–1180. IEEE.
- Lin, J.; Liu, D.; Li, H.; and Wu, F. 2020. M-LVC: Multiple frames prediction for learned video compression. In *Proc. IEEE Comput. Soc. Conf. Comput. Vis. Pattern Recognit*, 3546–3554.
- Lin, J.; Liu, D.; Liang, J.; Li, H.; and Wu, F. 2021a. A Deeply Modulated Scheme for Variable-Rate Video Compression. In *IEEE Int. Conf. on Image Process.*, 3722–3726. IEEE.
- Lin, J.; Liu, D.; Liang, J.; Li, H.; and Wu, F. 2021b. Modulated Variable-Rate Deep Video Compression. In *2021 Data Compression Conference (DCC)*, 351–351. IEEE.
- Liu, F.; and Chen, Z. 2021. Multi-Objective Optimization of Quality in VVC Rate Control for Low-Delay Video Coding. *IEEE Trans. Image Process.*, 30: 4706–4718.
- Lu, G.; Cai, C.; Zhang, X.; Chen, L.; Ouyang, W.; Xu, D.; and Gao, Z. 2020a. Content adaptive and error propagation aware deep video compression. In *European Conference on Computer Vision*, 456–472. Springer.
- Lu, G.; Ouyang, W.; Xu, D.; Zhang, X.; Cai, C.; and Gao, Z. 2019. Dvc: An end-to-end deep video compression framework. In *Proc. IEEE Comput. Soc. Conf. Comput. Vis. Pattern Recognit*, 11006–11015.
- Lu, G.; Zhang, X.; Ouyang, W.; Chen, L.; Gao, Z.; and Xu, D. 2020b. An end-to-end learning framework for video compression. *IEEE Trans. Pattern Anal. Mach. Intell.*, 43(10): 3292–3308.
- Mao, Y.; Wang, M.; Wang, S.; and Kwong, S. 2021. High Efficiency Rate Control for Versatile Video Coding Based on Composite Cauchy Distribution. *IEEE Trans. Circuits Syst. Video Technol.*, 32(4): 2371–2384.
- Marino, J.; Yue, Y.; and Mandt, S. 2018. Iterative amortized inference. In *Int. Conf. on Machine Learning*, 3403–3412. PMLR.
- Mentzer, F.; Agustsson, E.; Tschannen, M.; Timofte, R.; and Van Gool, L. 2019. Practical Full Resolution Learned Lossless Image Compression. In *Proc. IEEE Comput. Soc. Conf. Comput. Vis. Pattern Recognit*.
- Mercat, A.; Viitanen, M.; and Vanne, J. 2020. UVG dataset: 50/120fps 4K sequences for video codec analysis and development. In *Proceedings of the 11th ACM Multimedia Systems Conference*, 297–302.
- Minnen, D.; Ballé, J.; and Toderici, G. D. 2018. Joint autoregressive and hierarchical priors for learned image compression. *Advances in neural information processing systems*, 31.
- Mohamed, S.; Rosca, M.; Figurnov, M.; and Mnih, A. 2020. Monte Carlo Gradient Estimation in Machine Learning. *J. Mach. Learn. Res.*, 21(132): 1–62.
- Sheng, X.; Li, J.; Li, B.; Li, L.; Liu, D.; and Lu, Y. 2021. Temporal Context Mining for Learned Video Compression. *arXiv preprint arXiv:2111.13850*.
- Sun, Z.; Tan, Z.; Sun, X.; Zhang, F.; Li, D.; Qian, Y.; and Li, H. 2021. Spatiotemporal Entropy Model is All You Need for Learned Video Compression. *arXiv preprint arXiv:2104.06083*.

Tagliasacchi, M.; Valenzise, G.; and Tubaro, S. 2008. Minimum variance optimal rate allocation for multiplexed H. 264/AVC bit-streams. *IEEE Trans. Image Process.*, 17(7): 1129–1143.

van Rozendaal, T.; Huijben, I. A.; and Cohen, T. S. 2021. Overfitting for fun and profit: Instance-adaptive data compression. *arXiv preprint arXiv:2101.08687*.

Yang, R.; Yang, Y.; Marino, J.; and Mandt, S. 2020. Hierarchical autoregressive modeling for neural video compression. *arXiv preprint arXiv:2010.10258*.

Yang, Y.; Bamler, R.; and Mandt, S. 2020. Improving inference for neural image compression. *Advances in Neural Information Processing Systems*, 33: 573–584.

Yilmaz, M. A.; and Tekalp, A. M. 2021. End-to-End Rate-Distortion Optimized Learned Hierarchical Bi-Directional Video Compression. *IEEE Trans. Image Process.*, 31: 974–983.

Zhao, J.; Li, B.; Li, J.; Xiong, R.; and Lu, Y. 2021. A Universal Encoder Rate Distortion Optimization Framework for Learned Compression. In *Proc. IEEE Comput. Soc. Conf. Comput. Vis. Pattern Recognit.*, 1880–1884.

Zou, N.; Zhang, H.; Cricri, F.; Tavakoli, H. R.; Lainema, J.; Hanuksela, M.; Aksu, E.; and Rahtu, E. 2020. L 2 C-Learning to Learn to Compress. In *2020 IEEE 22nd International Workshop on Multimedia Signal Processing (MMSP)*, 1–6. IEEE.

Appendix

A An Analysis of Traditional Bit Allocation based on Li et al. (2016)

In this section, we select Li et al. (2016) as a typical example of traditional bit allocation algorithm and explain it in detail. And we show how our approach generalizes Li et al. (2016) and Li et al. (2022).

Li et al. (2016) is a well-acknowledged work in bit allocation. It is adopted in the official reference software of H.265 as the default bit allocation algorithm. For clarity, we follow Li et al. (2016) to put λ before R_i instead of D_i . Note that the location of λ can be swapped easily by taking the reciprocal of it.

First, let’s start with the empirical R-D models defined by Li et al. (2016). The bit allocation scheme of Li et al. (2016) relies on three important empirical models. Eq. 18 models the relationship between frame distortion D_i and its rate R_i , where a, b are parameters. Eq. 19 is the rate dependency and Eq. 20 is the quality dependency, where ω_i is parameter. In Li et al. (2016) the rate dependency is ignored and the quality dependency is greatly simplified to a linear relationship. In our approach, we accurately compute them via gradient.

$$D_i = aR_i^{-b}, \forall i = 1, \dots, K \quad (18)$$

$$\frac{\partial R_j}{\partial R_i} \approx 0, \forall i \neq j \quad (19)$$

$$\frac{\partial \sum_{j=i}^K D_j}{\partial D_i} \approx \omega_i, \forall i = 1, \dots, K \quad (20)$$

Li et al. (2016) derives the D - λ relationship and R - λ relationship (Eq. 21 and Eq. 22) from the fact that $\lambda_i = -\partial D_i / \partial R_i$ (essentially the same as Eq. 5) and Eq. 18. In our approach, we can easily compute their exact numerical

value through computational graph. However, it is not necessary as we adopt the latent y_i as the intermediate variable between R, D instead of λ .

$$R_i = \left(\frac{\lambda_i}{ab}\right)^{-\frac{1}{b+1}}$$

$$D_i = a\left(\frac{\lambda_i}{ab}\right)^{\frac{b}{b+1}} \quad (21)$$

$$\frac{\partial R_i}{\partial \lambda_i} = \left(\frac{1}{ab}\right)^{-\frac{1}{b+1}} \left(-\frac{1}{b+1}\right) \lambda_i^{-\frac{b+2}{b+1}}$$

$$\frac{\partial D_i}{\partial \lambda_i} = a\left(\frac{1}{ab}\right)^{\frac{b}{b+1}} \left(\frac{b}{b+1}\right) \lambda_i^{-\frac{1}{b+1}} \quad (22)$$

The frame-level bit allocation controls the bitrate of i^{th} frame by λ_i and optimizes the overall R-D cost controlled by λ_0 . In other words, its optimization target is as Eq. 23 (essentially the same as Eq. 3).

$$\lambda_1^*, \dots, \lambda_K^* \leftarrow \arg \min \lambda_0 \sum_{i=1}^K R_i + \sum_{i=1}^K D_i \quad (23)$$

And for each frame, the encoding parameters ϕ_i are optimized to minimize the local R-D cost (essentially the same as Eq. 1):

$$\phi_i^* \leftarrow \arg \min \lambda_i R_i + D_i \quad (24)$$

To solve Eq. 24, we can set the gradient of λ_i with regard to R-D cost to 0 (essentially the same as Eq. 4):

$$\lambda_0 \frac{\partial \sum_{j=i}^K R_j}{\partial \lambda_i} + \frac{\partial \sum_{j=i}^K D_j}{\partial \lambda_i} = 0, \forall i = 1, \dots, K \quad (25)$$

Then, we can take expand Eq. 25 and take Eq. 19 into it:

$$\begin{aligned} & \lambda_0 \frac{\partial \sum_{j=i}^K R_j}{\partial R_i} \frac{\partial R_i}{\partial \lambda_i} + \frac{\partial \sum_{j=i}^K D_j}{\partial D_i} \frac{\partial D_i}{\partial \lambda_i} \\ &= \lambda_0 \frac{\partial R_i}{\partial \lambda_i} + \frac{\partial \sum_{j=i}^K D_j}{\partial D_i} \frac{\partial D_i}{\partial \lambda_i} \\ &\approx 0 \end{aligned} \quad (26)$$

And then, we can solve λ_i by taking Eq. 20, 21, 22 into Eq. 26 as:

$$\lambda_i = \frac{\lambda_0}{\frac{\partial \sum_{j=i}^K D_j}{\partial D_i}} = \omega_i \lambda_0 \quad (27)$$

Where ω_i in Eq. 27 is a constant for each frame type (I, P, B frame). By now, we have completed the frame-level bit allocation of Li et al. (2016). It is optimal given the correctness of the empirical model Eq. 18, Eq. 19 and Eq. 20. However, those oversimplified empirical model makes it suboptimal in R-D performance when adopted to NVC (See Sec. 4.3).

Moreover, if we take $\lambda'_i = 1/\lambda_i, \lambda'_0 = 1/\lambda_0$ and take them into Eq. 27, we have Eq. 28, which is the scalar version of our explicit λ_i^* with $\partial R_{i \neq j} / \partial R_j = 0$. In other words, Li et al. (2016) can be regarded as a special case of our bit allocation, with extra assumption $\partial R_{i \neq j} / \partial R_j = 0$. Similarly, our bit allocation is also a generalization of Li et al.

(2022), which adopts a slightly different $\partial D_j/\partial D_i$ model and solves λ_i as Eq. 29.

$$\lambda'_i = \left(\frac{\partial \sum_{j=i}^K D_j}{\partial D_i} \right) \lambda'_0 \quad (28)$$

$$\lambda'_i = \left(1 + \sum_{j=i+1}^K \prod_{k=i+1}^j \frac{\partial D_k}{\partial D_{k-1}} \right) \lambda'_0 \quad (29)$$

B More on Online Encoder Update (OEU)

B.1 Why OEU is a Frame-level Bit Allocation

The online encoder update (OEU) of Lu et al. (2020a) is proposed to resolve the error propagation. It fits into the line of works on encoder over-fitting (Zou et al. 2020; van Rozen daal, Huijben, and Cohen 2021) and does not fit into the SAVI framework. However, it can be seen as an intermediate point between fully-amortized variational inference (FAVI) and SAVI: FAVI uses the same inference model parameter ϕ for all frames; SAVI performs stochastic variational inference on variational posterior parameter \mathbf{y}_i per frame, which is the finest-granularity finetune possible for latent variable model; And Lu et al. (2020a) finetune inference model parameter ϕ_i per-frame. It is less computational expensive but also performs worse compared with our method based on SAVI (See Tab. 3). However, it is more computational expensive and performs better compared with FAVI (or NVC without bit allocation).

	DVC	OEU	Proposed
Parameter	-	ϕ_i	\mathbf{y}_i, Δ_i
Granularity	-	frame-level	pixel-level
# of parameter	0	$\Theta(K \phi)$	$\Theta(KHW)$
# of encoder pass	1	$\Theta(T)$	1
# of decoder pass	0	$\Theta(T)$	$\Theta(T)$
T required	0	≈ 50	≈ 2000
R-D performance	poor	middle	good
Encoding time	fast	middle	slow
Decoding time	same	same	same

Table 3: A comparison between DVC (FAVI, w/o bit allocation), OEU (Lu et al. 2020a) and our proposed bit allocation (SAVI) approach. K is the GoP size, $|\phi|$ is the number of encoder parameters, $H \times W$ is the number of pixels, T is number of iteration.

Although OEU does not fit into SAVI framework, still it can be written as Eq. 30 and Eq. 31, which is very similar to our SAVI-based implicit bit allocation with Δ_i removed and optimization target changed from \mathbf{y}_i, Δ_i to encoder parameter ϕ_i .

$$\phi_{1:K}^* \leftarrow \arg \max_{\phi_{1:K}} \mathcal{L}^{BA} \quad (30)$$

$$\mathcal{L}^{BA} = \sum_i^K \underbrace{\log P_{\theta_{\lambda_0}}(\lfloor \mathbf{y}_i \rfloor | \lfloor \mathbf{y}_{<i} \rfloor)}_{-R_i} - \lambda_0 \sum_i^K \underbrace{d(\mathbf{x}, g_{\theta_{\lambda_0}}(\lfloor \mathbf{y}_{\leq i} \rfloor))}_{D_i} \quad (31)$$

This similarity also implies that Lu et al. (2020a) is optimized towards the overall bit allocation target. Thus, it is also an optimal bit allocation. However, the encoder parameter ϕ_i is only sensitive to the location of a frame inside a GoP. It can not sense the pixel location and pixel-level reference structure. So the bit allocation of Lu et al. (2020a) is limited to frame-level instead of pixel-level like ours.

Despite it is not pixel-level optimal bit allocation, OEU (Lu et al. 2020a) is indeed the true pioneer of bit allocation in NVC. However, the authors of Lu et al. (2020a) have not mentioned the concept of bit allocation in the original paper, which makes it a secret pioneer of bit allocation for NVC until now.

B.2 Why OEU is not an Error Propagation Aware Strategy

One problem of NVC is that the frame quality drops rapidly with the frame index t inside the GoP. Many works call this phenomena error propagation (Lu et al. 2020a; Sun et al. 2021; Sheng et al. 2021), including the OEU. And the error propagation aware technique is subtly related to bit allocation.

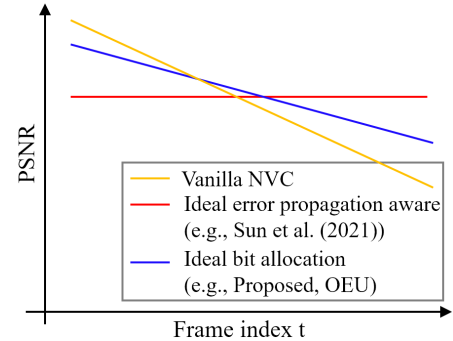


Figure 7: The comparison between ideal error propagation aware and ideal bit allocation.

In this paper, we would like to distinguish error propagation aware technique and bit allocation formally: error propagation aware technique aims to solve the problem of quality drop with frame index t , and an ideal solution to error propagation should produce a horizontal quality- t curve, just like the red line in Fig. 7. And Sun et al. (2021) aim to solve error propagation instead of bit allocation, as their frame quality is consistent to frame index t . However, the aim of bit allocation is to produce the best average R-D cost. And due to the frame reference structure, the frame quality of ideal bit allocation should drop with frame index t . As a result, the quality degrading rate of ideal bit allocation is less steep than vanilla NVC, but it almost never falls horizontal.

From the old school bitrate control’s perspective (Tagliasacchi, Valenzise, and Tubaro 2008), the target of avoiding error propagation is *minVar*, which means that we want to minimize the quality fluctuation between frames. On the other hand, the target of bit allocation is *minAvg*, which means that we want to minimize the average distortion under constrain of bitrate. And usually, those two targets are in odd with each other.

However, the results of a crippled error propagation aware method and an optimal bit allocation are similar: the degradation speed of quality-*t* curve is decreased but not flattened. And thus, sometimes the result of an optimal bit allocation is likely to be recognised as an unsuccessful error propagation aware method. This similarity has disorientated Lu et al. (2020a) to falsely classify themselves into error propagation aware strategy instead of bit allocation.

As we empirically show in Fig. 14, the quality-*t* curves of both our proposed method and OEU are not horizontal. Instead, they are just less steep than the original DVC (Lu et al. 2019). This phenomena further verifies that OEU is essentially a bit allocation, instead of an error propagation aware strategy.

B.3 Why the Reproduced OEU Result is Slightly Different from the Original Paper

The result of the reproduced OEU (Lu et al. 2020a) in Tab. 1 is around 0.2dB lower than the original paper in terms of BD-PSNR. And this is likely to stem from the difference in I frame model and I frame λ . First, we adopt Cheng et al. (2020) as I frame model and the original OEU paper (Lu et al. 2020a) adopts Ballé et al. (2018) as I frame model. Second, for the four R-D trade-off points $\lambda_0 = \{256, 512, 1024, 2048\}$, we set the I frame’s $\lambda_I = 255^2 \times \{0.0067, 0.0130, 0.0250, 0.0483\} = \{436, 845, 1626, 3141\}$, with pretrained models provided by Bégaïnt et al. (2020). On the other hand, the original paper of OEU adopts $\lambda_I = \{1024, 2048, 4096, 12000\}$, which is obviously very different from our setting.

To simulate the original paper of OEU as much as possible, we conduct an extra reproduction of OEU using Ballé et al. (2018) as I frame. We select $\lambda_I = 255^2 \times \{0.025, 0.048, 0.09, 0.18\} = \{1625, 3140, 5852, 11704\}$. Note that there is still quite some distance between the λ_I s as we do not have their I frame models at hand. And we are using the pretrained models with λ s as close as possible. The second round reproduction result is shown in Fig. 8 and Tab. 4. We see that the original OEU paper reports the BD-PSNR of 0.71dB. (Note that no actual number is given in the original paper, and we manually trace the R-D curve of Fig. 9 in the original OEU paper. And only the result on HEVC Class C is given by the original paper.) The reproduction with Cheng et al. (2020) as I frame has BD-PSNR of 0.49 (As Tab. 1) and the reproduction with Ballé et al. (2018) as I frame has BD-PSNR of 0.59. In fact, this is already pretty close to the original paper. We think the extra distance (around 0.1dB) might lies in the mismatch of λ_I . Note that this range of fluctuation does not harm our central claim, as the BD-PSNR of our proposed approach is 1.11dB, which is 0.4dB higher compared with 0.71dB.

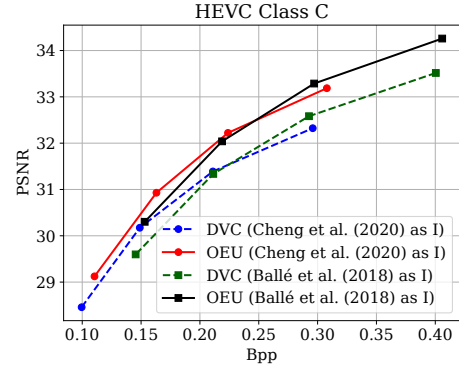


Figure 8: Reproduced results of Lu et al. (2020a) with different I frame models.

	BD-PSNR(dB)
Original OEU paper (Lu et al. 2020a)	0.71
Reproduced with Cheng et al. (2020) as I	0.49
Reproduced with Ballé et al. (2018) as I	0.59

Table 4: A comparison between original OEU (Lu et al. 2020a) and our reproduction with different I frame models on HEVC Class C dataset.

C More on Exact R-D Model

C.1 Proof of Thm. 2

Proof. Proof sketch: First, we will solve λ_i^* of Eq. 3 analytically with the precise R-D model defined by the computational graph. And then we will proof Thm. 2 by showing that $\lambda_i^* = \lambda_i'$.

Similar to how we expand Eq. 11, we first expand $\partial R_j / \partial \lambda_i, \partial D_j / \partial \lambda_i$ as Eq. 32 given the precise R-D model Eq. 15:

$$\begin{aligned} \frac{\partial R_j}{\partial \lambda_i} &= \prod_{k=i+1}^j \frac{\partial R_k}{\partial R_{k-1}} \frac{\partial R_i}{\partial \lambda_i} \\ \frac{\partial D_j}{\partial \lambda_i} &= \prod_{k=i+1}^j \frac{\partial D_k}{\partial D_{k-1}} \frac{\partial D_i}{\partial \lambda_i} \end{aligned} \quad (32)$$

Then by taking Eq. 32 into Eq. 4, we obtain Eq. 33:

$$\begin{aligned} & \left(1 + \sum_{j=i+1}^K \prod_{k=i+1}^j \frac{\partial R_k}{\partial R_{k-1}}\right) \frac{\partial R_i}{\partial \lambda_i} + \\ & \lambda_0^T \left(1 + \sum_{j=i+1}^K \prod_{k=i+1}^j \frac{\partial D_k}{\partial D_{k-1}}\right) \frac{\partial D_i}{\partial \lambda_i} = 0 \end{aligned} \quad (33)$$

Further, multiply each side of Eq. 33 by $\partial \lambda_i / \partial D_i$ and

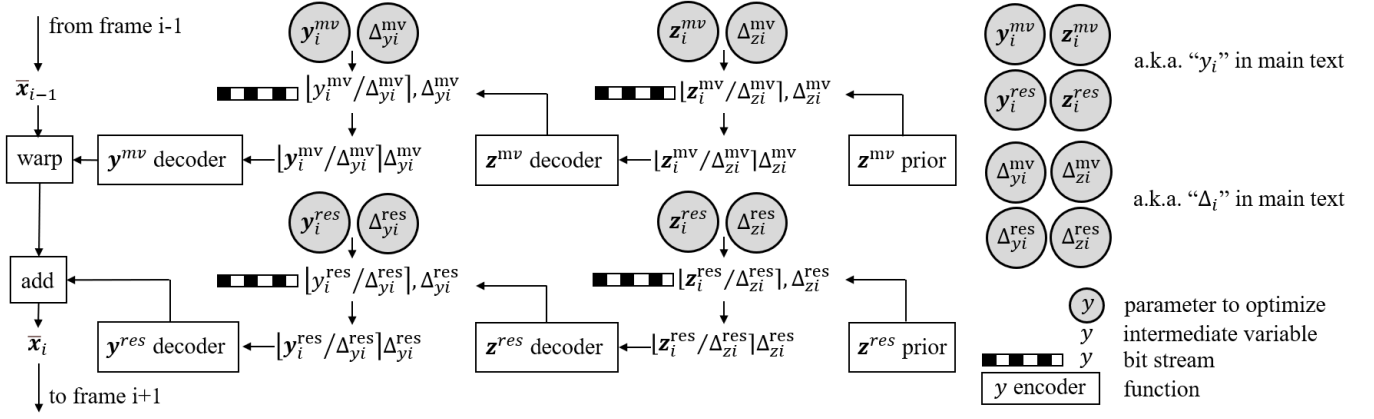


Figure 9: Overall framework of detailed implementation based on DVC (Lu et al. 2019). The DCVC’s (Li, Li, and Lu 2021) framework is very similar.

take Eq. 5 into it, we have Eq. 34:

$$\begin{aligned}
& -(1 + \sum_{j=i+1}^K \prod_{k=i+1}^j \frac{\partial R_k}{\partial R_{k-1}}) \lambda_i^{*T} + \\
& \lambda_0^T (1 + \sum_{j=i+1}^K \prod_{k=i+1}^j \frac{\partial D_k}{\partial D_{k-1}}) = 0 \quad (34)
\end{aligned}$$

Then immediately, we have Eq. 35 holds, which proofs Thm. 2.

$$\begin{aligned}
\lambda_i^* &= (1 + \sum_{j=i+1}^K \prod_{k=i+1}^j \frac{\partial D_k}{\partial D_{k-1}})^T \lambda_0 \\
& / (1 + \sum_{j=i+1}^K \prod_{k=i+1}^j \frac{\partial R_k}{\partial R_{k-1}}) \\
& = \lambda_i' \quad (35)
\end{aligned}$$

□

C.2 Extending Exact R-D Model to General Case

In Sec 2.5, we give the form of exact R-D model for NVC with only P frames. In this section we extend it to any frame types. By doing so, we also extend Thm. 1 and Thm. 2 to general cases.

Consider the dense reference case when i^{th} frame can refer to all previous frames, which generalizes all other frame types. We can define the precise R-D model under such condition by following recursion:

$$\begin{aligned}
\frac{dR_j}{dy_i} &= \sum_{l=i}^{j-1} \frac{\partial R_j}{\partial R_l} \frac{dR_l}{dy_i} \\
\frac{dD_j}{dy_i} &= \sum_{l=i}^{j-1} \frac{\partial D_j}{\partial D_l} \frac{dD_l}{dy_i} \quad (36)
\end{aligned}$$

, where dy/dx represents the total derivative and $\partial y/\partial x$ represents the partial derivative. Previously we have not distinguished these two concepts as our computational graph is simple enough.

It is important to note that naively recursively expanding Eq.36 by its definition is intractable. However, an obvious dynamic programming scheme can reduce the complexity into $\Theta(K^3)$, where K is the GoP size, so long as we recognise that we can construct a memorized array of $dR_j/dy_i, dD_j/dy_i$. And by expanding this recursive definition on P frame cases (only $\partial R_{l+1}/\partial R_l \neq 0$ and $\partial D_{l+1}/\partial D_l \neq 0$), we can obtain Eq. 14. Moreover, we can easily extend Thm. 1 and Thm. 2 to general frame type by substituting Eq. 14 with Eq. 36.

D More Experiments

D.1 Detailed Framework for Implementation

In the main text and analysis, we use y_i to abstractly represent all the latent and Δ_i to abstractly represent all the quantization step size for frame i . While for DVC (Lu et al. 2019) and DCVC (Li, Li, and Lu 2021), the actual bit-stream is divided into four parts: the first level of residual latent y_i^{res} , the second level of residual latent z_i^{res} , the first level of optical flow latent y_i^{mv} , and the second level of optical flow latent z_i^{mv} . This is shown in the overall framework diagram as Fig. 9. In the main text $y_i = \{y_i^{res}, z_i^{res}, y_i^{mv}, z_i^{mv}\}$. And in our bit implementation and allocation, each of the four latent has their corresponding quantization step size: $\Delta_{iy}^{res}, \Delta_{iz}^{res}, \Delta_{iy}^{mv}, \Delta_{iz}^{mv}$. In the main text $\Delta_i = \{\Delta_{iy}^{res}, \Delta_{iz}^{res}, \Delta_{iy}^{mv}, \Delta_{iz}^{mv}\}$.

Despite that we write y_i, Δ_i as optimization parameter, in practice only $y_i^{res}, z_i^{res}, \Delta_{iy}^{res}$ is involved in the optimization. And $\Delta_{iz}^{res}, y_i^{mv}, z_i^{mv}, \Delta_{iy}^{mv}, \Delta_{iz}^{mv}$ are fixed during bit allocation. As in the early stage of this paper, we empirically find that optimizing Δ_{iz}^{res} with gradient based optimization makes training unstable, and optimizing motion related parameters $y_i^{mv}, z_i^{mv}, \Delta_{iy}^{mv}, \Delta_{iz}^{mv}$ makes R-D performance worse (See Tab. 5). The preliminary intuition is that the gradient variance with regard to Δ_{iz}^{res} could be high, and

the optimization of latent of optical flow may also have gradient difficulty.

	R (bpp.)	D (MSE)	R-D cost
Initial	1.9277	4.36e-3	10.8621
Joint optimization	1.7239	4.85e-3	11.6521

Table 5: Experimental results of jointly optimize motion latent \mathbf{y}^{mv} , \mathbf{z}^{mv} and residual latent \mathbf{y}^{res} , \mathbf{z}^{res} on HEVC Class D dataset with the target $\lambda = 2048$. The joint optimization increases R-D cost.

D.2 Detailed Experimental Settings

For all the experiments unless specified, we select the $\lambda_0 = \{256, 512, 1024, 2048\}$, which follows the convention of baselines (Lu et al. 2019; Li, Li, and Lu 2021). For I frames, we set the $\lambda_I = 255^2 \times \{0.0067, 0.0130, 0.0250, 0.0483\} = \{436, 845, 1626, 3141\}$, with pretrained models provided by Bégaïnt et al. (2020). Note that the λ_I looks strange as CompressAI provides pretrained model of Cheng et al. (2020) with λ s defined with pixel range $[0 - 1]$. While the DVC and DCVC provide pretrained model with λ s defined with pixel range $[0 - 255]$. For HEVC CTC Class B and UVG with DVC (Lu et al. 2019) as baseline, we train our approach and Lu et al. (2020a) by slicing the original sequences into 640×640 blocks to save GPU memory. Similarly, for HEVC CTC Class B/E and UVG with DCVC (Li, Li, and Lu 2021) as baseline, we train our approach and Lu et al. (2020a) by slicing the original sequences into 640×640 blocks to save GPU memory. No decoder model in this paper is trained from scratch, so we do not have a training dataset or experimental setting for model training.

D.3 More Results on Bit Implementation

Variable Bitrate Coding In Fig. 2, the single decoder of green line is trained with $\lambda_0 = 1024$, and the bit implementation target λ is $\{128, 256, 512, 1024, 2048, 4096\}$. The 4 decoders of the red line are trained with $\lambda_0 = \{256, 512, 1024, 2048\}$, and the bit implementation target λ is $\{0.75, 0.875, 1.0, 1.125, 1.25\} \times \lambda_0$. The red line is the upper convex hull of the R-D points.

Note that we have not compared to any other bit implementation methods, such as Lin et al. (2021a,b), because it has nothing to do with our claim. We only claim results on bit allocation. And we only want to verify that the usability of bit implementation is reasonable. It is quite possible that other bit implementation methods outperform ours, but they can not be extended into the implicit bit allocation approach.

Pixel-level Bit Implementation Fig. 10 shows more pixel-level bit allocation results on HEVC Class B. The obvious checkerboard pattern on bit distribution map indicates the effectiveness of our method. However, the difference between the frames seems to be below just noticeable difference (JND), and the qualitative results are not that obvious.

Similarly, we have not compared to any other pixel-level bit implementation methods, because that has nothing to do

with our claim. We only claim results on bit allocation. And we only want to verify that the usability of pixel-level bit implementation is reasonable. Although we might be the first to consider pixel-level bit implementation for NVC, our results are not strong enough to support a separate claim.

D.4 More Results on Bit Allocation

More Quantitative Results Fig. 12 shows the R-D curves of the proposed bit allocation compared with baselines (w/o bit allocation) and OEU (Lu et al. 2020a) on HEVC Class B/C/D/E and UVG dataset.

Qualitative Results Moreover, we show the qualitative results of bit allocation in Fig. 16, Fig. 17 and Fig. 18. We can see that our approach not only improve quantitative result, but also significantly enhanced the perceptual quality of video compared with the baseline.

Entropy Coding Verification To ensure the soundness of our approach, we verify it with real arithmetic coding, and the results are shown in Fig. 11. We can see that the distance between theoretical bitrate (computed by entropy) and actual bitrate (length of bitstream from arithmetic coder) is negligible (≈ 0.0001 bpp).

Error Bar Fig. 13 and Tab. 6 shows the standard deviation σ and mean μ of rate and distortion (Lu et al. 2020a) over 5 random trials. It can be observed that both our method and OEU are not sensitive to randomness. This is not surprising as the base models are pre-trained, and the randomness of our method and OEU has nothing to do with model initialization, but only lies in stochastic gradient descent. And Fig. 13 shows that the distance between OEU and our method is far beyond $1 \times \sigma$ on each side.

	λ	bpp		PSNR	
		μ	σ	μ	σ
Proposed	256	0.130	7.64e-4	29.56	0.0157
	512	0.197	9.15e-4	31.41	0.0136
	1024	0.270	7.12e-4	32.68	8.46e-3
	2048	0.382	1.18e-3	33.40	8.61e-3
OEU	256	0.115	3.97e-4	28.71	0.0637
	512	0.173	5.21e-4	30.63	0.0133
	1024	0.243	4.65e-4	31.94	0.0126
	2048	0.334	7.31e-4	32.97	7.64e-3

Table 6: Error bar of proposed method and OEU (Lu et al. 2020a) on HEVC Class D dataset.

D.5 More Analysis

Fig. 15 is a supplementary of Fig. 6. It shows the bitrate distribution change of other sequences in HEVC Class E.

Fig. 14 shows how the quality (PSNR), bitrate and R-D cost change with the frame index t within a GoP. It is interesting to see that as frame index increases, the PSNR of proposed method and OEU drops in general, which is intuitively correct considering the frame reference structure.

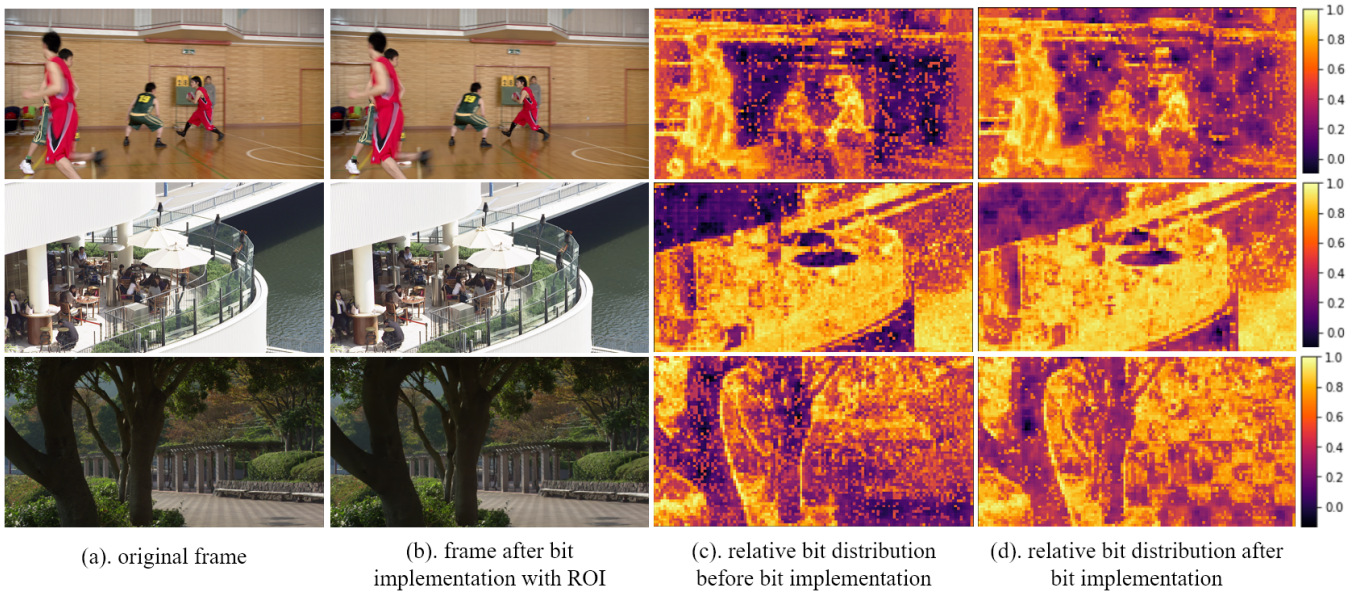


Figure 10: More pixel-level bit allocation results on HEVC Class B. The ROI map is the same checkerboard map as Fig. 4.

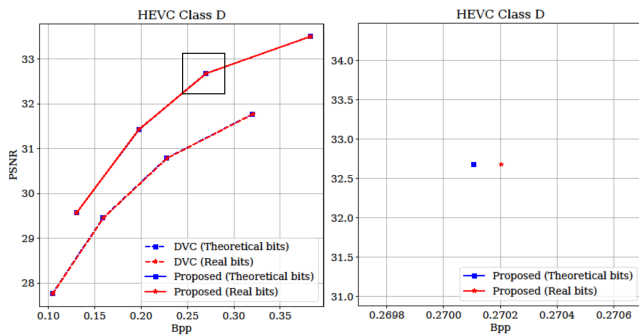


Figure 11: Experimental results of entropy coding verification on HEVC Class D dataset.

As the precedent frames are more referred, they should have best quality. It is also interesting to see that the I frame’s R-D cost of OEU and proposed approach is significantly higher than DVC, while the P frame’s R-D cost of OEU and proposed approach is significantly lower than DVC. This is due to the bit allocation: The algorithms are allocating more bitrate to I frame, so as to improve the quality of subsequent frames. The DVC’s choice of I frame λ is somewhat arbitrary. The original paper (Lu et al. 2019) seems to choose a I frame with λ larger than the P frame, which is an inaccurate bit allocation, and our bit allocation and OEU successfully amend it.

More interestingly, the frame with highest quality is the I frame ($t = 0$) for DVC (Lu et al. 2019). However, the frame with highest quality is the 2^{nd} P frame ($t = 2$) for both OEU (Lu et al. 2020a) and the proposed approach, which is also the result of bit allocation.

E More Discussions

Another less obvious limitation is that our approach is only explainable when D_i factorizes with pixels. For example, when distortion is measured in MSE. However, when distortion is measured with non-factorized metrics such as MS-SSIM/LPIPS, it becomes complicated to define pixel-level bit allocation itself. While from the optimization target’s perspective, the result of bit allocation remains optimal.

Despite the pixel-level bit implementation is obvious by looking at the bitrate distribution result, the reconstructed image is less obvious. It might have something to do with the autoregressive context of Cheng et al. (2020). The autoregressive context of Cheng et al. (2020) is a mini-size bit allocation with-in I frame. And this internal bit allocation might intervene our bit implementation.

In addition, which parameter to include in optimization remains under-explored. Problems such as, why optimizing the quantization step size of second level latent causes unstable training, remain unsolved. Future works should be called to address those issues, probably from gradient variance and optimization perspective.

Ethical Statement

Improving the R-D performance of NVC has valuable social impact. First, better R-D performance means less resources required for video storage and transmission. Considering the amount of video produced everyday, it is beneficial to the environment if we could save those resources by improving codec. Second, the traditional codec requires dedicated hardware decoder for efficient decoding, while NVC could utilize the universal neural accelerator. The improvement of neural codec can be readily deployed without hardware up-gradation.

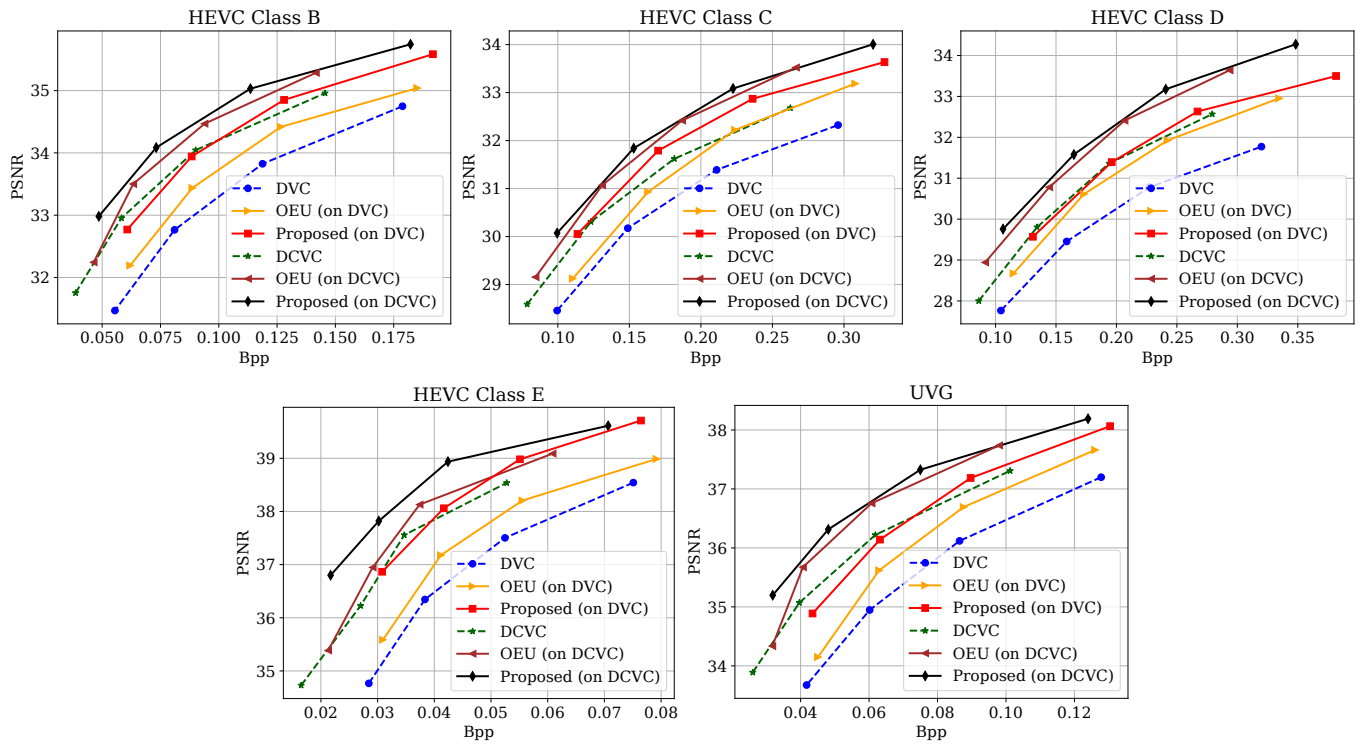


Figure 12: The R-D performance of our bit allocation compared with baselines (w/o bit allocation) and OEU.

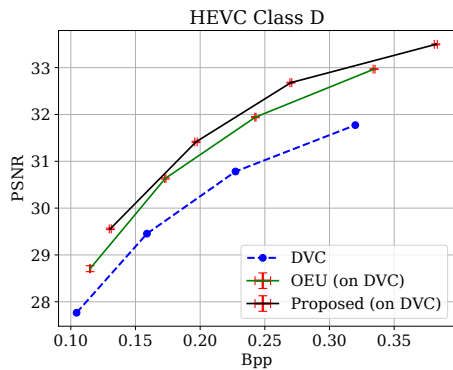


Figure 13: Mean and standard deviation of proposed method and OEU (Lu et al. 2020a) on HEVC Class D dataset. No error bar of DVC baseline is reported as we use the pre-trained model directly. The red bars represent $\pm\sigma$.

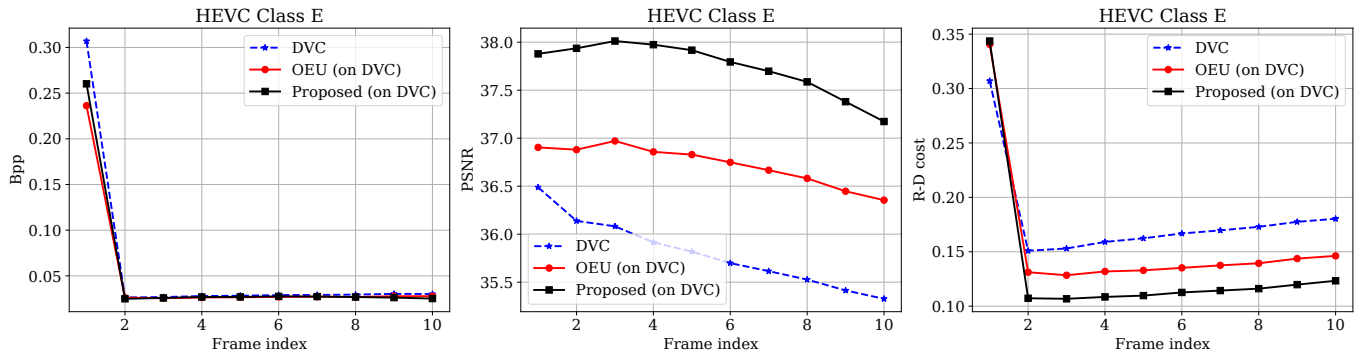


Figure 14: The change of bpp, PSNR and R-D cost with time inside a GoP on *FourPeople* in HEVC Class E dataset.

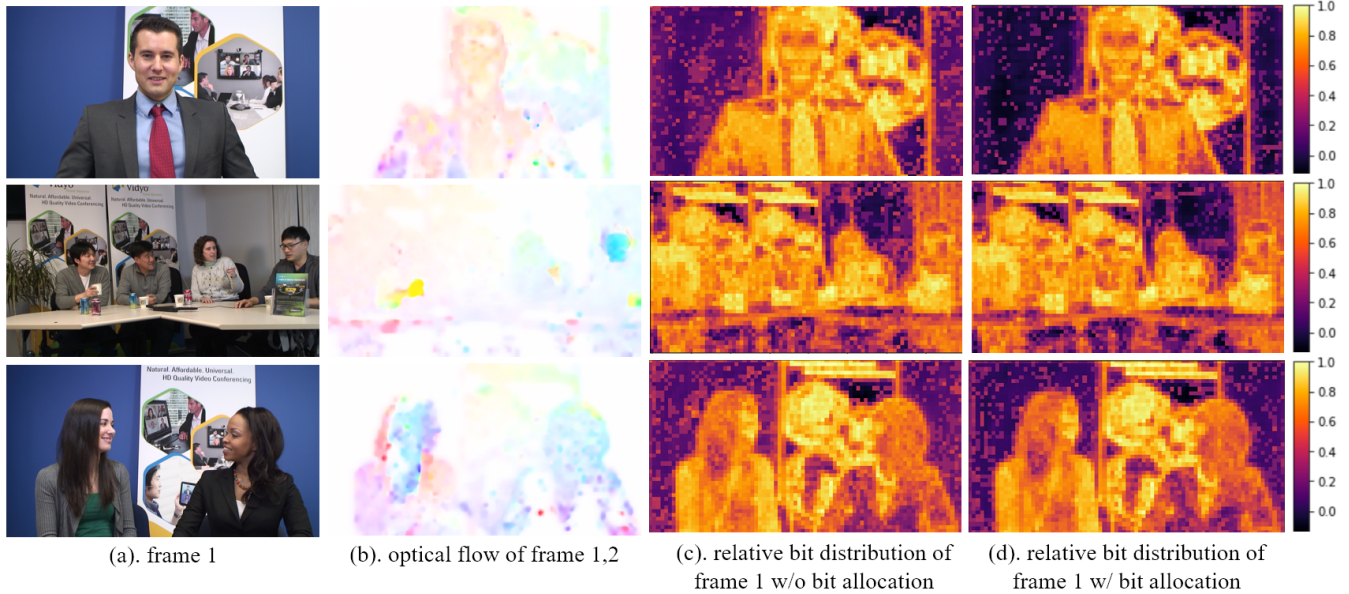
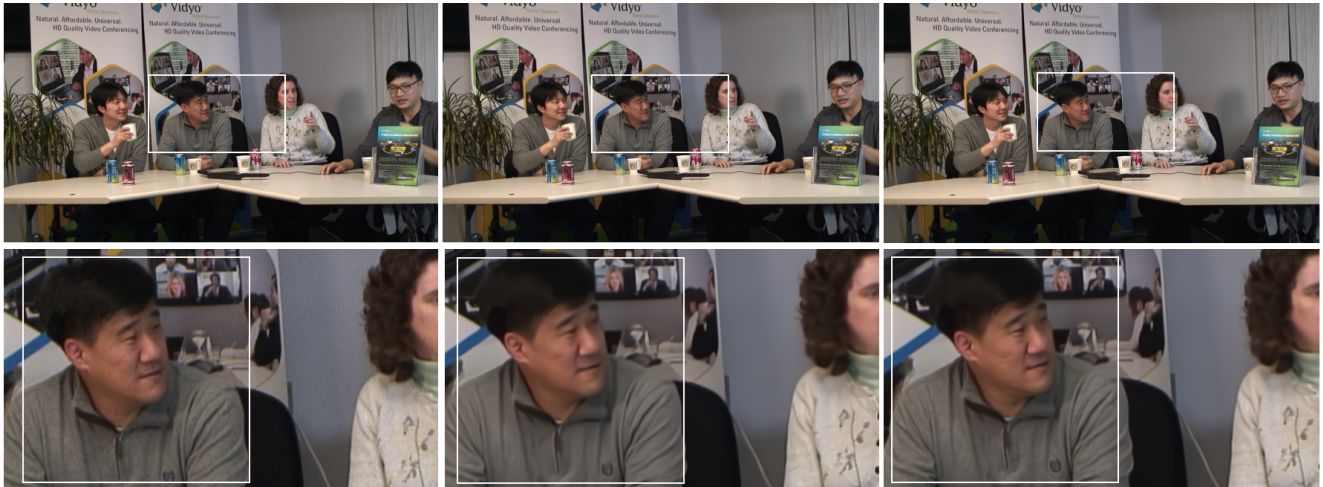


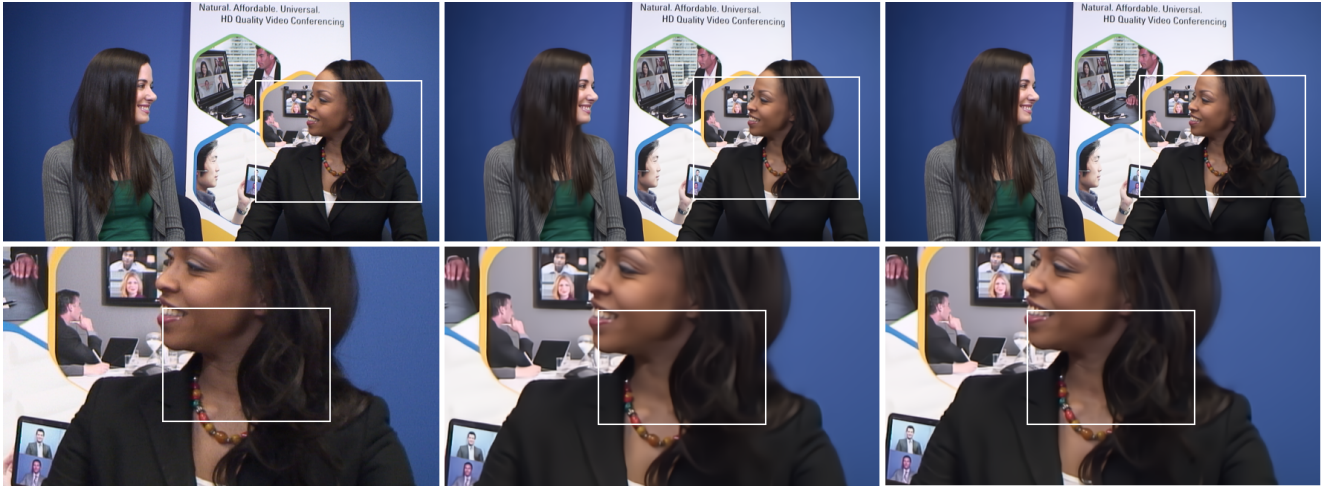
Figure 15: The bit rate distribution before and after bit allocation of HEVC Class E dataset.



(a). original frame

(b). before bit allocation
bpp: 0.0625, PSNR: 37.66 db.

(b). after bit allocation
bpp: 0.0406, PSNR: 39.12 db.



(a). original frame

(b). before bit allocation
bpp: 0.0394, PSNR: 37.14 db.

(b). after bit allocation
bpp: 0.0296, PSNR: 38.67 db.

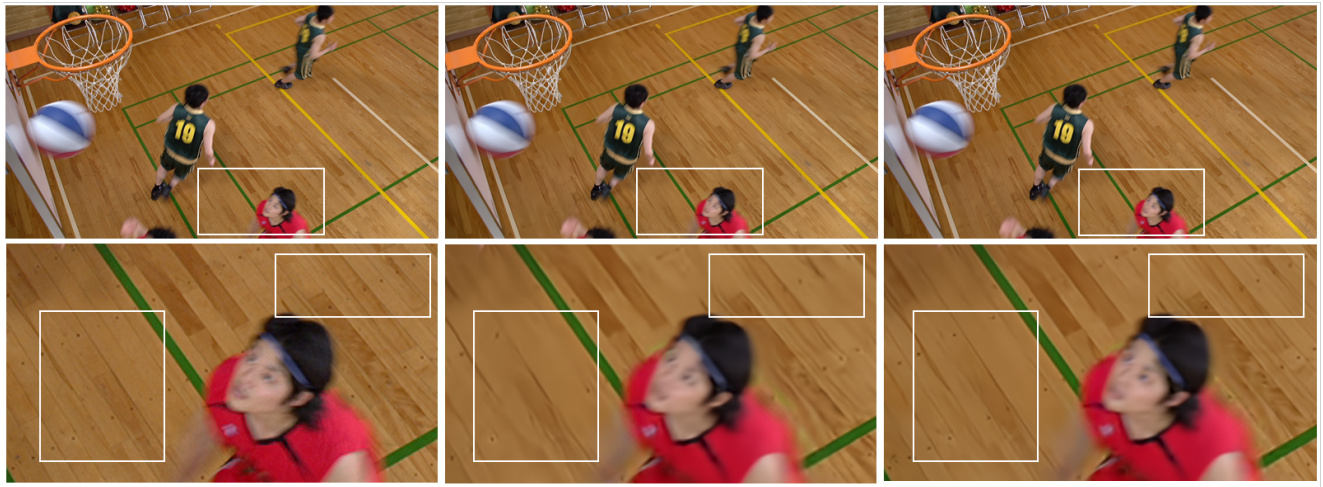


(a). original frame

(b). before bit allocation
bpp: 0.0356, PSNR: 37.25 db.

(b). after bit allocation
bpp: 0.0271, PSNR: 38.73 db.

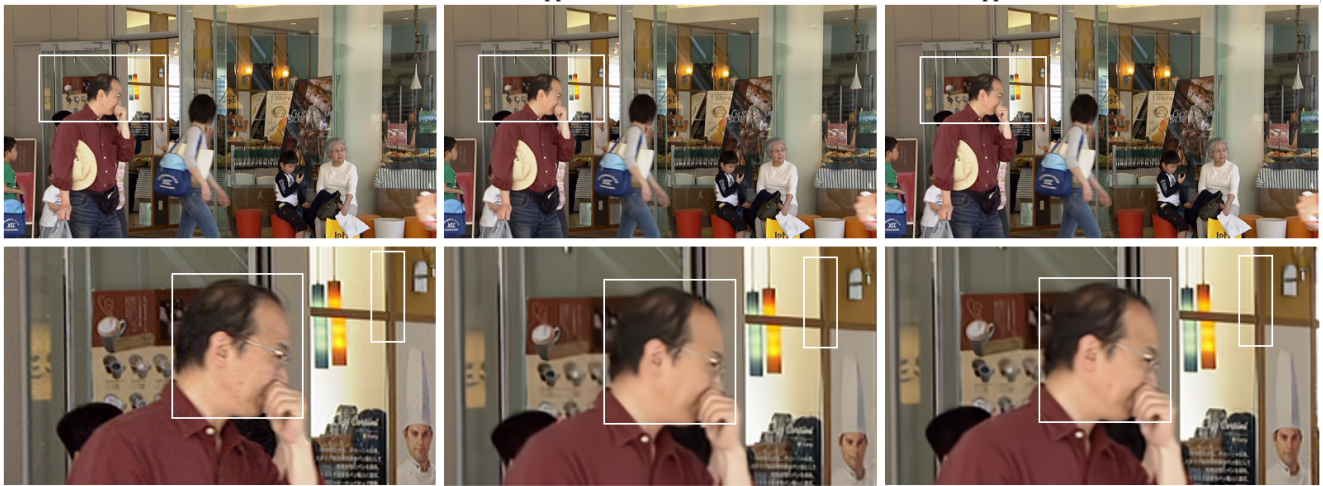
Figure 16: Qualitative results of bit allocation on HEVC Class E. The baseline approach is DVC (Lu et al. 2019).



(a). original frame

(b). before bit allocation
bpp: 0.097, PSNR: 33.13 db.

(b). after bit allocation
bpp: 0.121, PSNR: 34.97 db.



(a). original frame

(b). before bit allocation
bpp: 0.101, PSNR: 32.33 db.

(b). after bit allocation
bpp: 0.071, PSNR: 34.29 db.

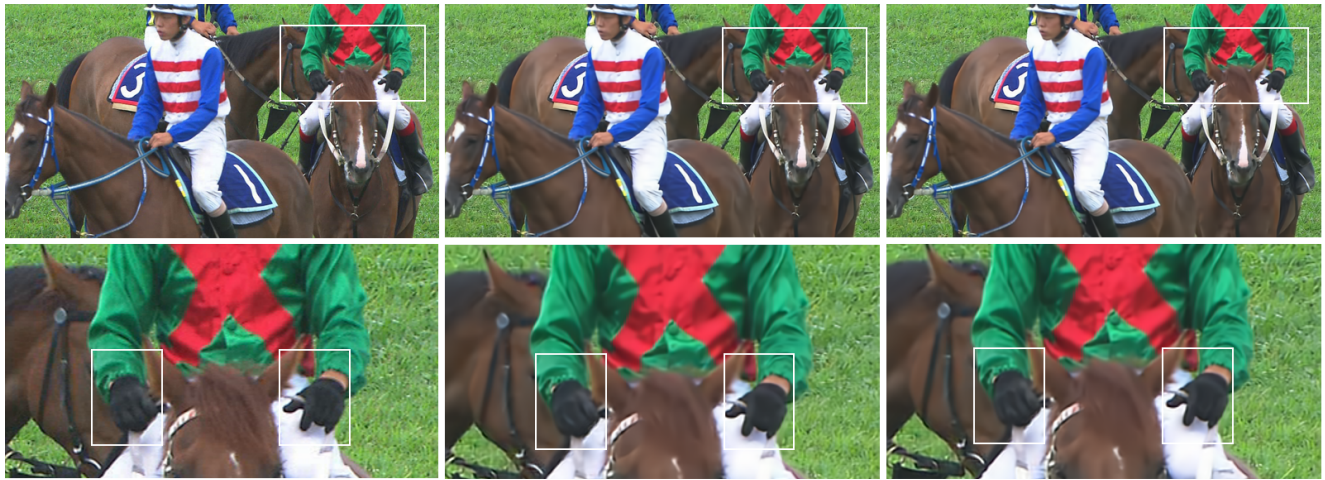


(a). original frame

(b). before bit allocation
bpp: 0.246, PSNR: 27.41 db.

(b). after bit allocation
bpp: 0.205, PSNR: 29.04 db.

Figure 17: Qualitative results of bit allocation on HEVC Class C Part I. The baseline approach is DVC (Lu et al. 2019).



(a). original frame

(b). before bit allocation
bpp: 0.251, PSNR: 30.22 db.

(b). after bit allocation
bpp: 0.221, PSNR: 31.43 db.

Figure 18: Qualitative results of bit allocation on HEVC Class C Part II. The baseline approach is DVC (Lu et al. 2019).